

Perturbations to the system

5.1 Introduction

Ice core records reveal that the concentration of CO₂ in the Earth's atmosphere ($x\text{CO}_2$) has undergone substantial fluctuations over the course of the late Quaternary [Petit *et al.*, 1999]. That the climatic system in general has undergone parallel excursions, with glacial periods characterized by extensive northern hemisphere ice sheets occurring contemporaneously with low $x\text{CO}_2$ suggests that there is a fundamental causal link between the two. Should changes in $x\text{CO}_2$ be at least partly responsible for driving the global climate system there would be obvious repercussions for our predictions for the coming decades of the radiative forcing effects due to anthropogenic CO₂ emissions. Even if over the glacial-interglacial cycles atmospheric composition responded in a predominantly passive manner, then elucidation of the mechanisms involved is still vital to our understanding of key feedbacks operating in the present-day Earth system [Falkowski *et al.*, 2000].

The sheer diversity and biogeochemical scope of mechanisms purporting to explain low glacial levels of CO₂ has made any comparative assessment within a single framework problematic, with models often customized around a single process. Hypotheses range from relatively simple changes in surface ocean biological productivity [Knox and McElroy, 1984; Martin, 1990; Rich *et al.*, 1999; Sarmiento and Toggweiler, 1984], ocean circulation [Keir, 1988; Siegenthaler and Wenk, 1984; Toggweiler, 1999], and changes in the storage on continental shelves of nutrients and CaCO₃ [Berger, 1982a; Broecker, 1982; Opdyke and Walker, 1992; Shaffer, 1990], through subtle effects on deep-sea sediments exerted by changes in the particulate composition of biogenic material exported out of the euphotic zone [Archer and Maier-Reimer, 1994], to more exotic mechanisms such as transients in ocean pH driven by rapid manganese depositional events [Mangini *et al.*, 1991] and CH₄ out-gassing [Loehle, 1993]. However, of the mechanisms forwarded to date, when taken in isolation all fall short of simultaneously meeting constraints dictated by the various marine, terrestrial, and ice core paleoclimatic records [Broecker and Henderson, 1998; Holligan and Robertson, 1995]. It is thus becoming increasingly obvious that in spite of the perhaps aesthetic desirability of a single mechanism yet to be discovered and able to completely solve the mystery, the solution to the observed glacial-interglacial variability in $x\text{CO}_2$ almost certainly lies in a combination of processes operating during the late Quaternary. The problem then lies in determining the important mechanisms involved and constraining their relative overall contribution to the dynamics of the system. A series of potentially important mechanisms will therefore be characterized in isolation within the same model framework (SUE) and then combined together in a 'best guess' scenario. Although a number of comparative studies have been carried out in the past, these all have shared a common approach, of contrasting two steady states of the system: one characterized by modern (pre-industrial) boundary conditions and the other by those thought to be representative of the Last Glacial Maximum (LGM). Partly as a consequence of this, many of these studies (particularly those based around simple box model representations of the ocean) have concluded that permutations which give rise to a simile of glacial atmospheric and ocean chemistry are relatively easy to construct [Hausman and McElroy, 1999; Keir, 1988; Marino *et al.*, 1992; Toggweiler, 1999]. However, recent work based around a comprehensive OGCM-based global carbon cycle model has suggested that we are still far from solving the problem [Archer *et al.*, 2000]. In an attempt to increase the utilization efficiency of information available from both ice cores and the paleoceanographic record in constraining the operation of the global carbon cycle, mechanisms are tested on a dynamical (i.e., time-stepping) basis. Changes in the boundary conditions of the global carbon cycle are reconstructed for multiple glacial-interglacial cycles so that the dynamical evolution of the system may be followed over that entire period. Special emphasis will be placed on the role of the Southern Ocean, particularly with respect to the inception of deglacial transitions in the system.

5.2 Evidence for glacial-interglacial variability of the global carbon cycle

The primary records of past change in the global carbon cycle over the course of the late Quaternary comes from ice cores. Material (both solid and gaseous) contained within the crystalline structure of accumulating ice in both low latitude glaciers [Thompson *et al.*, 1995] and high latitude ice caps [Edwards *et al.*, 1998; Jouzel *et al.*, 1995; Petit *et al.*, 1999; Smith *et al.*, 1999] present us with a proxy record of past climate. While cores located in low latitude glaciers rarely extend back even as far as the LGM, the greater ice thickness afforded by high latitude ice caps generally allows a much longer record to be obtained, with records obtained to date spanning almost 250 ka in Greenland [Johnsen *et al.*, 1997], but back as far as 420 ka BP in Antarctica [Petit *et al.*, 1997, 1999]. With respect to the past state of the global carbon cycle the most important single indicator is the concentration of CO₂ held within bubbles trapped within the ice. Such bubbles start to form in the firn relatively near the surface, effectively recording a snapshot of atmospheric composition at the time of occlusion [Oeschger *et al.*, 1984]. However, Greenland ice contains high concentrations of aeolian carbonate-rich dust, which can chemically denature over time thereby contaminating trapped air samples with CO₂ produced *in situ* [Indermühle *et al.*, 1999; Smith *et al.*, 1997]. Therefore they cannot be relied upon as indicators of a changing carbon cycle. In contrast, the low carbonate content of Antarctic ice suggests that cores recovered there will record past CO₂ concentrations with much greater fidelity [Smith *et al.*, 1997]. The ice core record from Vostok (78°S, 106°E, elevation 3,488 m) covering the last ~400 ka [Petit *et al.*, 1999] will be used to provide the model target for glacial-interglacial variability in $x\text{CO}_2$.

A second property of atmospheric composition recorded in ice cores and of direct relevance to the state of the global carbon cycle at any point in time is the stable isotopic composition of CO₂ ($\delta^{13}\text{C}^{\text{CO}_2}$). The ~27 ka long record from Taylor Dome [Smith *et al.*, 1999] will be used to provide the model target for variability in this. Visual inspection suggests that the age scales constructed for the Vostok and Taylor Dome cores do not exactly correspond. A simple linear age transformation (reduction in gas age of 7.5%) is therefore made to the Taylor Dome CO₂ record so that it matches that at Vostok over the most recent deglacial transition (Figure 5-1a). As a result of considerable analytical difficulties inherent in measuring isotopic composition of ice core $\delta^{13}\text{C}^{\text{CO}_2}$ [Leuenberger *et al.*, 1992; Smith *et al.*, 1999] there is a considerable degree of uncertainty in the values obtained. Confidence in many of the major features of this record can be improved, however, through reference to estimates of past (atmospheric) isotopic composition made by an entirely independent method, based on preserved samples of the shrub *Atriplex confertifolia* [Marino *et al.*, 1992]. The ¹⁴C-derived age scale for *A. confertifolia* is adjusted so that major transitions are in phase with recorded events at Taylor Dome, as shown in Figure 5-1b. It can be seen that while the magnitude of some of the events disagree, many of the

general features are held in common between the two records. In particular, there is a pronounced negative $\delta^{13}\text{C}^{\text{CO}_2}$ anomaly during the initial stages of Termination I, with a second one around the time of the Younger Dryas (~12.8 ka BP [Blunier *et al.*, 1997]). The presence of this first anomaly is also supported by planktonic foraminiferal $\delta^{13}\text{C}$ records which exhibit contemporaneous features, similar in magnitude to cores located between the Antarctic polar and subtropical fronts in the Southern Ocean [Ninnemann and Charles, 1999] but slightly more muted than cores from the eastern tropical Pacific and tropical Atlantic [Curry and Crowley, 1987; Shackleton *et al.*, 1983].

Another effective integrator of the state of the global carbon cycle for which there is extensive (paleoceanographic) information available concerns the CaCO₃ lysocline transition zone. The CaCO₃ content of benthic sediments is primarily a function of deep ocean pH together with particulate matter rain rates. Changes in the shape and depth of the CaCO₃ lysocline transition zone, therefore, represents a powerful constraint upon the operation of the majority of mechanisms forwarded to explain the observed variability in $x\text{CO}_2$. Sediment cores located in the Pacific Ocean indicate that CaCO₃ was more abundant during glacial than interglacial times there; LGM time-slice reconstructions show a slightly greater areal extent of CaCO₃-rich sediments [Catubig *et al.*, 1998] while lysocline sections detail glacial age lysoclines lying of order 500 m deeper [Berger, 1978, 1982b; Farrell and Prell, 1989, 1991; Karin *et al.*, 1992]. In contrast, distribution patterns of sediments in the Atlantic basin exhibit significantly lower CaCO₃ abundances than during glacial periods [Balsam and McCoy, 1987; Catubig *et al.*, 1998]. This is supported by estimates made of the location of the calcite lysocline during glacial periods which suggest it was some 200-700 m deeper [Berger, 1968; Crowley, 1983], although some estimates put this shoaling as large as 1500 m or more in the western north Atlantic [Balsam, 1983]. Variability in the depth of the carbonate compensation depth (CCD) appears to be generally much more muted when compared to the response of the lysocline in either basin [Balsam, 1983; Farrell and Prell, 1989]. Thus, not only the depth of the lysocline but the shape of the entire transition zone must be altering in response to perturbations of the global carbon cycle. That some mechanisms (such as whole-ocean changes in pH) will tend to alter the depth of both the lysocline and CCD to a similar extent while others (such as changes in the CaCO₃:POC rain ratio [Archer and Maier-Reimer, 1994]) tend to shift lysocline depth whilst leaving the location of the CCD relatively invariant, may further aid in the elucidation of the key mechanisms involved.

There is a cornucopia of other paleoceanographic proxies reflecting changes in the earth system; for instance, in the relative abundance of solid sediment constituents (calcite, aragonite, opal, detrital material, organic matter), the isotopic ($\delta^{11}\text{B}$, $\delta^{13}\text{C}$, $\delta^{14}\text{C}$, $\delta^{15}\text{N}$, $\delta^{18}\text{O}$, $\delta^{30}\text{Si}$, $^{87}\text{Sr}/^{86}\text{Sr}$, $^{231}\text{Pa}/^{230}\text{Th}$) and chemical (Cd/Ca, Ge/Si, and Mg/Ca ratios) composition of these solid components, together with phytoplankton and zooplankton species abundance, marine and terrestrial biomarkers, the degree of shell fragmentation,

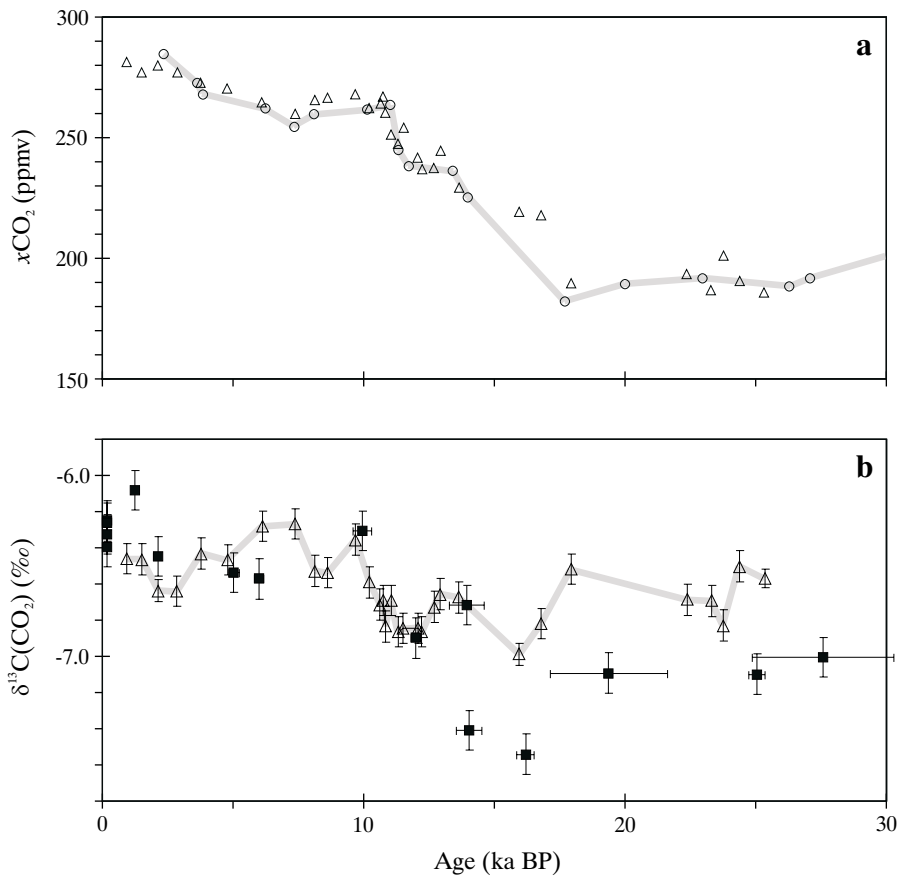


Figure 5-1 Comparisons between; (a) the CO₂ ice core records from Vostok (empty circles) [Petit *et al.*, 1999] and Taylor Dome (empty triangles) [Smith *et al.*, 1999] and transformed onto the Vostok age scale, (b) δ¹³C(CO₂) record from the Taylor dome ice core (empty triangles) and reconstructed from plant organic matter (filled squares) [Marino *et al.*, 1992], both on the Vostok age scale.

and varied burial fluxes (³He, Ba, Fe, Al, Zn, authigenic U). However, many of these depend on individual processes operating with the ocean not accounted for in the model and can be more localized in scope than the resolution of SUE1608 reasonably allows for. The implications of such proxies for this present study will therefore only be discussed where especially relevant to a particular mechanism or region of glacial-interglacial change.

for the relative importance of low vs high latitude regions in controlling xCO₂ indicate a fundamental divide separating box models from OGCMs [Archer *et al.*, in press; Broecker *et al.*, 1999a]. It is important to establish what class of response the models developed from use in this present study fall into, before either SUE1608 or SUE2108 can be wholly relied upon to critically assess mechanisms for glacial-interglacial change.

5.3 Uncertainties in model response to perturbations of the carbon cycle

Recent studies have questioned whether certain types of model can be relied upon to correctly predict the response of atmospheric composition to a perturbation applied to the system. In particular, attention has focussed on whether simple box-type models might over-estimate the sensitivity of xCO₂ to physical and biological changes located at high latitudes. The results of two independently-developed indices

5.3.1 The ‘Harvardton Bear Equilibrium Index’

Using an index (the ‘Harvardton Bear Equilibrium Index’, or ‘HBEI’) first devised by Bacastow [1996], Broecker *et al.* [1999a] found that global carbon cycle models based around a box-type representation of the ocean scored considerably lower (~0.11 for 2- and 3-box models and around 0.2 for ‘multi-box’ models) than those based around 3D OGCMs (up to 0.32). In this index (the ‘Warm Surface’ variant), higher values represent a greater relative equilibrium response of xCO₂ to a perturbation of the low latitude surface ocean. It was concluded from this that box models significantly overestimate the importance of high latitude

regions; the implication being that the results of early studies based upon such models, which suggested that low glacial $x\text{CO}_2$ is explicable through changes in Southern Ocean circulation and/or biological productivity, might be in error [Broecker *et al.*, 1999a]. Somewhat worryingly, the parent model from which both SUE1608 and SUE2108 derive their ocean structure and circulation, the Bern 2D ZOGCM [Stocker and Wright, 1996], scored an HBEI value of just 0.14, putting its response into a similar class to (and in fact below) the box models. Rather surprisingly, however, SUE1608 gives an HBEI score of just under 0.39, making atmospheric composition slightly less sensitive to high latitude perturbations even than in OGCM-based models. This apparently anomalous behaviour of the Bern 2D model is now investigated.

A new baseline model is constructed (designated 'SUE1608'), taking the same physical structure and advective field as SUE1608 (outlined in 4.2) but otherwise configured following Marchal *et al.* [1998b], the main features being: 18 time steps of 20 days each with no seasonality, CO_2 air-sea gas exchange with a uniform transfer rate of $0.067 \text{ mol m}^{-2} \text{ a}^{-1} \text{ ppmv}^{-1}$, no sea ice cover, new production derived by restoring ocean surface $[\text{PO}_4]$ towards observations at 30 m depth [Conkright *et al.*, 1994] on a time scale of 100 days with export production split 50:50 between DOM and POM phases, uniform vertical and horizontal eddy diffusivities of $0.2 \text{ cm}^2 \text{ s}^{-1}$ and $10 \times 10^6 \text{ cm}^2 \text{ s}^{-1}$, respectively, and with the system run entirely 'closed' (i.e., no sediment burial or weathering inputs). The HBEI value so obtained is 0.21, a little higher than that reported by Broecker *et al.* [1999a] for the full Bern 2D model, probably largely a result of

remaining differences in model resolution and biogeochemical schemes. With total export production fixed, a number of changes are made to the details of ocean mixing in SUE1608' and the HBEI value recalculated. These are summarized in Table 5-1.

From this sensitivity analysis it can be seen that the details of vertical and horizontal diffusivity have a relatively minor effect on the HBEI score (± 0.04). However, there is a strong dependence on the details of high latitude convection, with the introduction of just 5% mixing to a stratified high latitude ocean surface almost halving the HBEI score. This suggests that much of the variability in values reported by Broecker *et al.* [1999a] might be attributed to differences in the representation of convective mixing. Indeed, whether mixing takes place seasonally or uniformly all year around (for the same mean annual rate) can account for much of the difference between the seasonal Hamburg [Maier-Reimer, 1993] and the annual circulation Princeton [Murnane *et al.*, 1999] 3D OGCMs. Furthermore, the low HBEI value of the 'PANDORA' box model [Broecker and Peng, 1986] can be almost entirely explained by the relatively thick surface layer (~450 m) used. Other factors (not shown) such as the introduction of a wind speed dependency on air-sea CO_2 gas exchange, the presence of sea ice cover, and the absence of DOM production (equivalent to exacerbating nutrient trapping in equatorial up-welling regions) have relatively little effect.

Table 5-1 Sensitivity to Ocean Mixing of HBEI Value Scored by the Re-configured Baseline Model SUE1608'

Model details	HBEI value
SUE1608' (default)	0.21
SUE1608' - enhanced vertical diffusivity ¹	0.24
SUE1608' - enhanced ($200 \times 10^6 \text{ cm}^2 \text{ s}^{-1}$ at depth) horizontal eddy diffusivity	0.17
SUE1608' - 100% intensity convective adjustment (default)	0.21
SUE1608' - 50% intensity convective adjustment	0.22
SUE1608' - 25% intensity convective adjustment	0.23
SUE1608' - 10% intensity convective adjustment	0.26
SUE1608' - 5% intensity convective adjustment	0.30
SUE1608' - 0% intensity convective adjustment	0.49
SUE1608' - depth of all convective adjustment unrestricted (default)	0.21
SUE1608' - depth of all convective adjustment restricted to upper 1000 m (equivalent to the uppermost 5 layers)	0.22
SUE1608' - depth of all convective adjustment restricted to upper 500 m (equivalent to the uppermost 4 layers)	0.23
SUE1608' - depth of all convective adjustment restricted to upper 150 m (equivalent to the uppermost 3 layers)	0.35
SUE1608' - depth of all convective adjustment restricted to upper 100 m (equivalent to the uppermost 2 layers)	0.41
SUE1608' - depth of all convective adjustment completely restricted (i.e., none)	0.49

¹ Following Weaver and Sarachik [1991]

5.3.2 The ‘Archer Abiotic xCO₂’ test

In a contemporary study, David Archer investigated the potential bias that simpler ocean models might exhibit [Archer *et al.*, in press] in the relative strength of regional control on atmospheric composition. Various global carbon cycle models were run in an ‘abiotic’ mode and the steady state concentration of CO₂ in the atmosphere noted. A similar trend was apparent to that found by Broecker *et al.* [1999a], whereby 3-box and ‘multi-box’ models tended to cluster at one end of the scale with an abiotic xCO₂ value in the range ~220-230 ppmv, while most 3D OGCMs exhibited high values in the range 250-290 ppmv. Archer *et al.* [in press] deduced that it was low latitude vertical diffusivity in 3D OGCMs (not present in box models) that went towards overcoming the control exerted by deep water formation at high latitudes. They therefore concluded, similarly to Broecker *et al.* [1999a], that the importance of high latitudes in glacial xCO₂ draw-down (such as through Southern Ocean Fe fertilization) deduced from box models has been overstated. However, contrary to the results of the HBEI test, abiotic xCO₂ exhibited by the Bern 2D model (289 ppmv) places it firmly into the same group as the 3D OGCMs, supported by tests made with SUE1608 (287 ppmv). The factors controlling the value of this second index are also further investigated.

SUE was configured following a number of different published configurations, detailed in Table 5-2. The results of the abiotic xCO₂ test closely follow those of Archer *et al.* [in press]. Small (≤7 ppmv) differences do arise, possibly due to differences in the choices made for the carbonate dissociation constants. With the exception of the 3-box model (whose representation of only two surface boxes is a little too crude to translate to the real world), latitudinal and longitudinal boundaries are now assigned to each surface ocean region, chosen in order to both retain the surface areas of the original model and to be generally consistent with regional descriptions given of the surface boxes. SSTs are derived from Levitus *et al.* [1994c] using these boundaries (see 4.2.2) and the tests re-run. It can be seen (Table 5-2) that use of more realistic SSTs has a dramatic effect on multi-box model abiotic xCO₂ values, with that of ‘PANDORA’ now comparable to most (depth-coordinate) OGCMs, while ‘CYCLOPS’ only just falls short of isopycnic OGCMs [Archer *et al.*, in press]. This suggests that the apparent divide between box and OGCM-based carbon cycle

models dictated by this test may be partly an artefact of unrealistically low mean SSTs adopted in the original model definitions.

5.3.3 Implications for this present study

Under both the ‘HBEI’ and ‘Abiotic xCO₂’ tests of relative inter-regional control on atmospheric composition SUE1608 (as does SUE2108) scores similarly to carbon cycle models based upon 3D OGCMs. That the HBEI score is slightly on the high side suggests that the response of xCO₂ to perturbations occurring at high latitudes in SUE1608 may, if anything, be underestimated. There is thus little danger of seriously overstating the importance of high latitudes in this present study. In light of the strong control exerted by convective mixing regime on the sensitivity of the system to perturbations, it is important that convective adjustments are prevented from co-varying in order that the response of the atmosphere to specific mechanisms for low glacial xCO₂ might be isolated.

5.4 Model evaluation of mechanisms for glacial-interglacial xCO₂ variability

A variety of mechanisms purporting to explain the observed glacial-interglacial variability in the concentration of atmospheric CO₂ are now evaluated. However, there are several aspects of the operation of the global carbon cycle over the late Quaternary for which SUE1608 is not entirely suited for investigating. Changes in the balance between nitrogen supply (through its fixation from the atmosphere) and losses (through denitrification) are suspected to play an important role [McElroy, 1983; Shaffer, 1990]. However, the lack of explicit representation of the oceanic nitrogen cycle in SUE precludes such analysis. In addition, with the exception of the Atlantic overturning circulation, changes in ocean circulation will not be considered further in any detail.

One of the aims of the approach taken here is to consider the dynamical evolution of the global carbon cycle over the entirety of several glacial-interglacial cycles. For assessment of system response, the Vostok ice core provides a target record of fluctuations in the concentration of atmospheric CO₂ over the last ~400 ka [Petit *et al.*, 1999]. However, in

Table 5-2 ‘Abiotic xCO₂’ Values Exhibited by Various Configurations of SUE, and as a Function of SST Prescription

Model	Number of boxes - original configuration	SUE configuration - (as columns×layers)	xCO ₂ (ppmv); original SSTs	xCO ₂ (ppmv); adjusted SSTs	Reference
3-box	3	2×2	218	n/a	Sarmiento and Toggweiler [1984]
PANDORA	10	8×3	224	279	Broecker and Peng [1986]
CYCLOPS	13	6×3	230	249	Keir [1988]
Bern 2D ZOGCM	406	29×14	285	288	Stocker and Wright [1996]

order to generate a synthetic atmospheric record the model must be informed of changes in boundary conditions (e.g., physical ocean surface conditions, dissolved chemical or aeolian inputs) over a comparable period, i.e., the model must be continuously ‘forced’ for the duration of the simulation run. With the possible exception of the use of benthic oxygen isotopes as a proxy for sea level change, there is no continuous 400 ka record fully describing any suspected forcing of the system. Indeed, for many glacial-interglacial changes in boundary conditions such as SST, terrestrial carbon storage, or sea ice extent, there exist paleoclimatic reconstructions for only isolated periods (‘time slices’) [Adams *et al.*, 1990; CLIMAP, 1984]. Even then, the magnitude of regional change is often highly controversial [Crosta *et al.*, 1998b; Crowley, 1995, 2000]. Forcings (externally imposed changes in boundary condition) are therefore devised with the aid of continuous records spanning at least the last 400 ka which can taken to be first-order proxies for the timing and rate of forcing variability over this period. The absolute magnitude of change spanning the last deglacial transition (i.e., 19→0 ka BP) is taken directly from time slices reconstructed for modern (pre-industrial) and glacial (LGM) conditions. Model forcing over the complete 400 ka interval is then derived by linearly transforming the proxy signal so that its magnitude at 0 and 19 ka BP corresponds to the respective values given by the two time slices. Forcing signals are applied to the model at a resolution of 1 ka but subsequently (internally) linearly interpolated to an annual time step. As a consequence, SUE is not particularly suited for detailed investigation of millennial-scale changes such as Dansgaard-Oeschger [Dansgaard *et al.*, 1982] and Heinrich [Bond *et al.*, 1992] events, which will not be considered further in this study. In light of the phase differences exhibited by climatic changes as deduced from ice cores taken from Greenland and Antarctica [Blunier *et al.*, 1997, 1998; Broecker and Henderson, 1998; Kim *et al.*, 1998; Sowers *et al.*, 1991], it may not always be appropriate to use the same forcing template for both hemispheres. In such situations different proxy templates are assigned to each polar region. The relative influence of these signals is then diminished away from each pole according to a pair of weighting functions

$$\gamma_{(lat)}^N = \left(\cos\left(\frac{90 - lat}{2}\right) \right)^2 \quad (5-1 a)$$

$$\gamma_{(lat)}^S = \left(\cos\left(\frac{90 + lat}{2}\right) \right)^2 \quad (5-1 b)$$

where $\gamma_{(lat)}^N$ and $\gamma_{(lat)}^S$ are the weighting factors for changes in boundary conditions of the Northern Hemisphere (NH) and Southern Hemisphere (SH), respectively, both as a function of (northern) latitude (*lat*).

In the model investigations that follow, following a spin-up of 50 ka (sufficient to bring the sediment system largely into steady state), SUE1608 is run for a total of 500 ka, a period over which it is informed by a variable boundary condition (the model ‘forcing’). Although the Vostok CO₂ record

extends back only just beyond 400 ka BP [Petit *et al.*, 1999], the model is forced over the entire 500 ka run length. This allows the initial 100 ka of model run to be treated as an additional spin-up period, the aim of which is to allow the model to relax towards a quasi-steady state (the long-term mean about which the system oscillates over the course of the glacial-interglacial cycles). Indeed, it is probably prudent to regard about half of the entire model run in this manner (i.e., up until 250 ka BP), leaving the response to 3 individual deglacial transitions and 2 glacial inception available for comparison with observations. To avoid contaminating the direct effects of the mechanisms being tested through secondary perturbations arising through changes in non-advective ocean circulation to which the system is apparently extremely sensitive (see 5.3.3), convective regimes produced by the steady-state baseline model are applied and held invariant.

As a first-order assessment, four key indicators of the state of the global carbon cycle will be considered: the concentration of atmospheric CO₂ together with its ¹³C isotopic signature and the shape evolution of the calcite lysocline in both the Atlantic and Pacific basins. All these records are presented for the last 400 ka (with the exception of $\delta^{13}C^{CO_2}$, for which observational data is currently only available back to ~25 ka BP [Smith *et al.*, 1999]). The calcite lysoclines are reconstructed with the aid of a series of synthetic sediment cores separated in ocean depth by 100 m (see 3.3.2.3); one set located in the south Atlantic and the other in the south Pacific Ocean (both centred on 23.75°S).

5.4.1 Sea level

In response to the waxing and waning of ice sheets over the course of the late Quaternary there was significant associated variability in sea level height. Of all the processes suspected to exert any significant perturbatory effect on the global carbon cycle over this period, only past changes in sea level can be reconstructed with any accuracy. However, while these changes are reliably recorded by proxy indicators such as coral terraces [Adkins *et al.*, 1998; Fairbanks, 1989; Lambeck and Nakada, 1992; Stein *et al.*, 1993] and transgressions of shallow marine environments [Yokoyama *et al.*, 2000], these are only primarily available for events surrounding the two most recent glacial terminations. As an alternative, changes in the oxygen isotopic composition of benthic foraminiferal calcite has often been used as a proxy for global ice volume and thus for sea level [Munhoven and Francois, 1994, 1996; Walker and Opydyke, 1995].

There are three distinct effects on the (oceanic) global carbon cycle arising from sea level change;

- Since the solubility ratio of CaCO₃ is a sensitive function of pressure (Appendix I), glacial reduction in the ambient hydrostatic pressure at the surface of deep-sea sediments will drive enhanced CaCO₃ preservation and thus lead to the removal of DIC and ALK from the ocean in a 1:2 ratio, driving xCO_2 higher.
- During glacial periods of lower ocean volume, dissolved species such as DIC, ALK, and nutrients will all become more concentrated in the ocean. Increasing DIC and

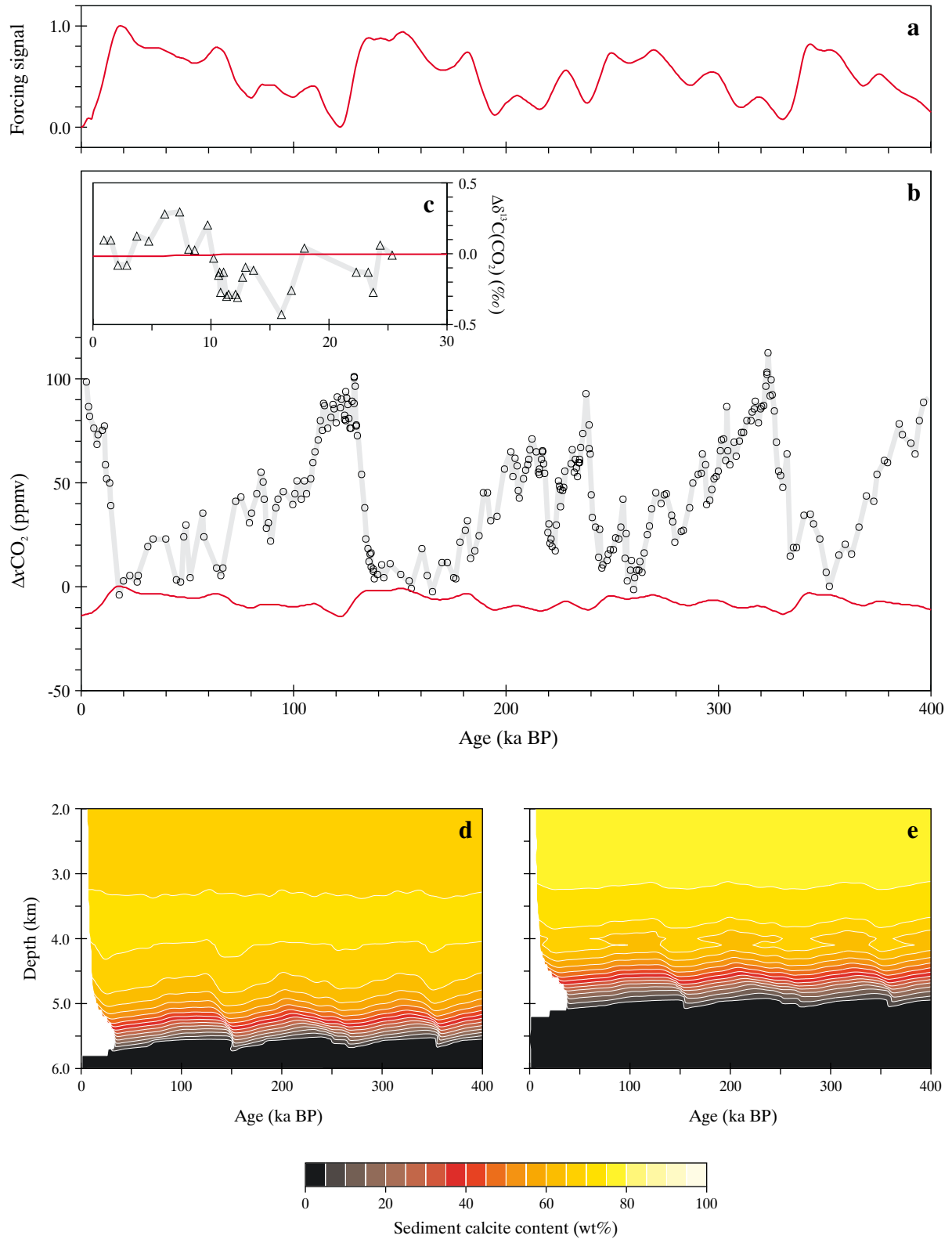


Figure 5-2 Effects on the global carbon cycle of glacial-interglacial variability in sea level. Shown are; (a) the forcing signal (normalized to a value of unity at the LGM); (b) model $x\text{CO}_2$ response (red line) compared to the Vostok ice core record [Petit *et al.*, 1999] (grey line with data points); (c) model $\delta^{13}\text{C}^{\text{CO}_2}$ response (red line) compared to the Taylor Dome ice core record [Smith *et al.*, 1999] (grey line with data points); (d) and (e) the response of the calcite lysocline in the (south) Atlantic and (south) Pacific basins, respectively.

ALK in a 1:1 ratio has the effect of driving $x\text{CO}_2$ up. However, complicating this response are further influences on $x\text{CO}_2$ related to increased export production and sedimentary opal preservation during glacial periods, both driven by the increased nutrient availability.

- Lastly, there is the effect of generally higher ocean salinity during glacials. This manifests itself (at least in terms of atmospheric composition) almost entirely through its influence on aqueous carbonate equilibria in the surface ocean, with an increase in salinity of 1‰ producing a typical increase in CO_2 fugacity ($f\text{CO}_2$) of order 10 ppmv.

The control that glacial-interglacial changes in sea level may have exerted on atmospheric composition is now tested. The SPECMAP stacked $\delta^{18}\text{O}$ record [Imbrie *et al.*, 1984] is used as a signal template for the reconstruction of sea level change over the last 400 ka. The magnitude of this signal is scaled by assuming that sea level just prior to Termination I was 117 m lower than at present [Fairbanks, 1989]. Since ocean volume is calculated directly from prescribed sea level in SUE and dissolved constituents in the ocean are considered inherently in mass unit terms, changes in oceanic tracer concentrations are automatically accounted for. Sea surface salinity (SSS) values are simply varied linearly with changes in sea level, resulting in a typical glacial enhancement in SSSs of $\sim 1\text{‰}$.

The results of this exercise are summarized in Figure 5-2. Deglacial sea level rise produces a decrease in $x\text{CO}_2$ of some 13.8 ppmv over the period 19→0 ka BP. This compares favourably with previous estimates for the magnitude of this effect of around 14 ppmv [Broecker and Peng, 1986]. Of the total change, decreasing SSSs are responsible for just under 50% via control exerted on surface ocean $f\text{CO}_2$, while the remaining processes tied to sea level change account for the rest. There is virtually no influence of sea level on $\delta^{13}\text{C}^{\text{CO}_2}$ ($<0.02\text{‰}$ over 19→0 ka BP). Perturbations in the lysocline transition zones in both Atlantic and Pacific basins is relatively modest (Figure 5-2d,e), with glacial deepening of ~ 300 and ~ 100 m, respectively. Around half of the Atlantic lysocline response and virtually the entirety of the Pacific response can be accounted for purely by changes in hydrostatic pressure. Although the sign of the change in the Atlantic basin is inconsistent with observations, the magnitude of the change is relatively small and thus could be easily masked by the operation of one or more additional mechanisms.

5.4.2 Ocean surface temperatures

Paleoclimatic reconstruction of the Earth's climate at the time of the LGM suggests that sea surface temperatures (SSTs) were significantly lower than today [CLIMAP, 1984]. Since temperature exerts a strong control on both the fugacity of CO_2 in ocean surface waters and on the degree of ^{13}C fractionation during air-sea gas exchange, it has been suggested that rising SSTs over the course of a deglacial transition could potentially account for much of the observed increase in both $x\text{CO}_2$ and $\delta^{13}\text{C}^{\text{CO}_2}$ [Bacastow, 1996;

Hofmann *et al.*, 1999; Stephens and Keeling, 2000]. As an initial test of the role that glacial-interglacial changes in SSTs may have played in altering atmospheric composition, spatially uniform changes in temperature are applied to the ocean surface taking LGM SSTs to be some 1.7°C lower than at present, consistent with estimates of mean global change [Broecker and Peng, 1986; Guilerson *et al.*, 1994]. Different signal templates are used to represent the differential climatic variability characterizing the two hemispheres. Northern latitudes are simply weighted via the SPECMAP curve [Imbrie *et al.*, 1984], while southern latitudes take information regarding the timing and rate of change of events from the Vostok δD record [Petit *et al.*, 1999] on the basis that changes in local (air) temperatures in continental Antarctica are strongly coupled with Southern Ocean SSTs [Sowers *et al.*, 1993].

The results of this exercise are summarized in Figure 5-3. The magnitude of the response of $x\text{CO}_2$ to the two separate forcings is comparable, with a 19→0 ka BP increase of 9.5 ppmv for SH-weighted SST changes and 7.2 ppmv weighted towards the NH. Differences between these arise only as a result of the shapes of the respective forcing signals, and due to the imbalance in the distribution of ocean surface area between the hemispheres. The combined $x\text{CO}_2$ deglacial rise is thus some 16.5 ppmv, a value which falls comfortably within the range 14-21 ppmv estimated from box models and 3D OGCMs for a similar global temperature change [Broecker and Peng, 1986, 1989; Heinze *et al.*, 1991]. Isotopic composition (Figure 5-3c) exhibits a 0.11‰ (19→0 ka BP) increase associated with SST changes weighted towards the SH and 0.08‰ to the north. The net deglacial increase in $\delta^{13}\text{C}^{\text{CO}_2}$ is then 0.19‰ . There is virtually no change in deep-sea sedimentary CaCO_3 (Figure 5-3d,e).

Glacial cooling at high latitudes was actually much more pronounced than nearer to the equator [CLIMAP, 1984]. A more realistic test of the effect of glacial-interglacial variability in SSTs on the global carbon cycle would be to consider inherent spatial heterogeneity in this change. The CLIMAP [CLIMAP, 1984] reconstructions of modern (pre-industrial) and LGM Earth surface conditions can be used to define this. However, recent studies based on paleoclimatic evidence from low latitudes such as from coral paleothermometers [Guilerson *et al.*, 1994] and high altitude air temperatures [Thompson *et al.*, 1995] suggest that the CLIMAP reconstruction may significantly underestimate glacial cooling in the tropics, although the precise degree of regional underestimation is highly controversial [Crowley, 2000]. A series of sensitivity tests are therefore carried out following Archer *et al.* [2000], with low latitude glacial SSTs progressively modified from their CLIMAP values. Three model runs are carried out. The first takes present-day and LGM ocean temperature distributions directly from CLIMAP. The second assumes tropical cooling at the time of the LGM was $\sim 2^\circ$ greater than suggested by CLIMAP, implemented in SUE1608 by reducing temperatures in each equatorial grid point by 2°C , with a 1°C reduction in the adjoining mid-latitude gyre regions (designated 'CLIMAP-2'). The third is similarly modified, but represents an end-member scenario of maximum likely change, with a

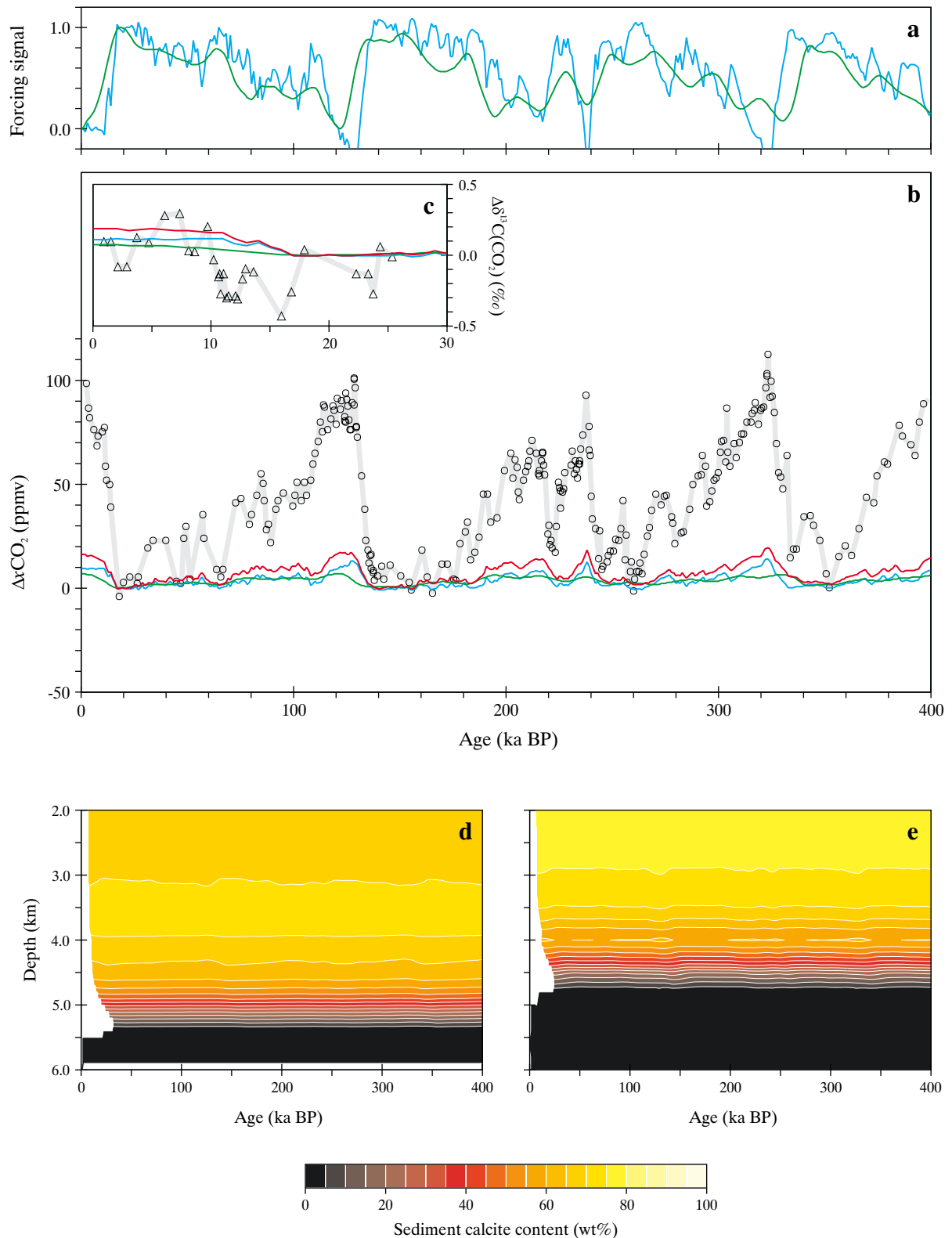


Figure 5-3 Effects on the global carbon cycle of glacial-interglacial variability in SST. Shown are; (a) the NH-weighted (green) and SH-weighted (blue) forcing signals; (b) model NH-weighted (green), SH-weighted (blue) and net (red) $\Delta x\text{CO}_2$ response compared to the Vostok ice core record [Petit et al., 1999] (grey line with data points); (c) model NH-weighted (green), SH-weighted (blue) and net (red) $\Delta\delta^{13}\text{C}^{\text{CO}_2}$ response compared to the Taylor Dome ice core record [Smüh et al., 1999] (grey line with data points); (d) and (e) the net response of the calcite lysocline in the (south) Atlantic and (south) Pacific basins, respectively.

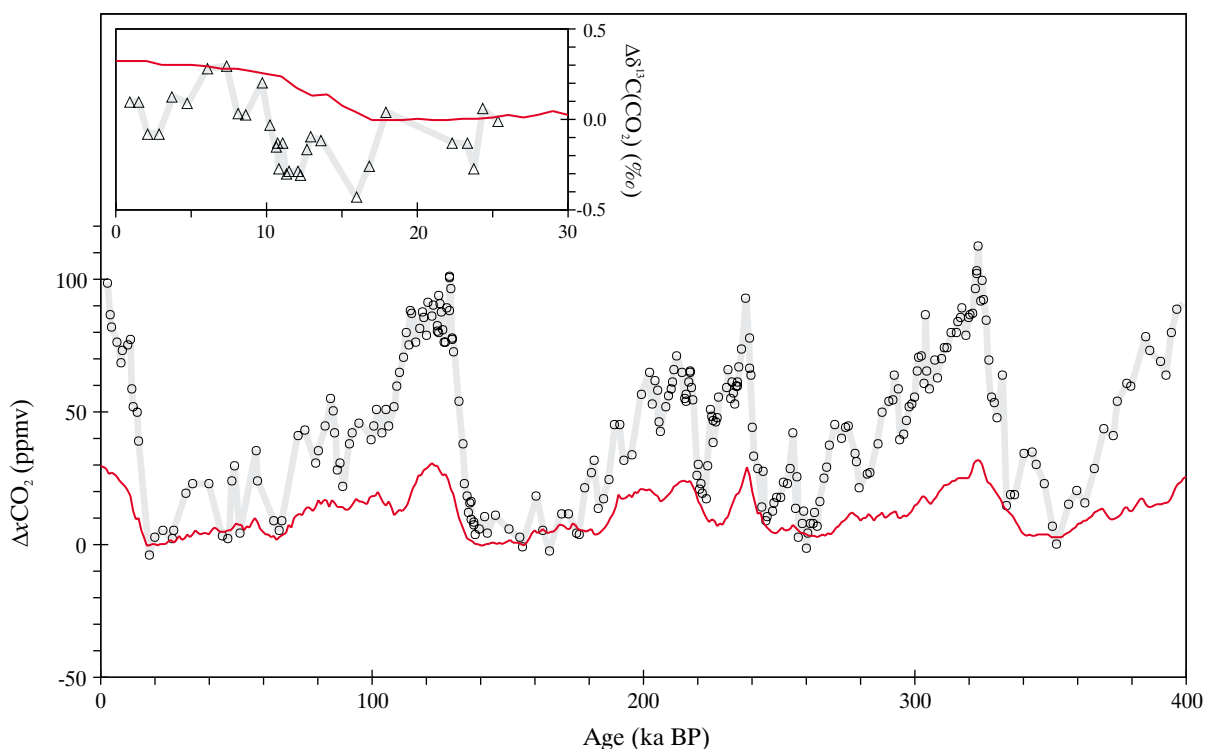


Figure 5-4 Effects on the global carbon cycle of glacial-interglacial variability in SST. Shown is the model $x\text{CO}_2$ response (red line) compared to the Vostok ice core record [Petit *et al.*, 1999] (grey line with data points) with inset – model $\delta^{13}\text{C}^{\text{CO}_2}$ response (red line) compared to the Taylor Dome ice core record [Smith *et al.*, 1999] (grey line with data points).

4°C tropical cooling and 2°C in the sub-tropics (designated ‘CLIMAP-4’).

The difference between the three CLIMAP-based scenarios is relatively small, with the model exhibiting a sensitivity to tropical SST changes of ~ 2 ppmv $^{\circ}\text{C}^{-1}$. This is slightly greater than the ~ 1 ppmv $^{\circ}\text{C}^{-1}$ reported by Archer *et al.* [2000], which might reflect differences between the respective model sensitivities to low latitude surface perturbations as highlighted by respective ‘HBEI’ scores (5.3.1). Alternatively, it may simply be an artefact arising from differences in model resolution with respect to how additional cooling is prescribed adjacent to the equatorial zones.

A glacial SST scenario similar to ‘CLIMAP-2’ is consistent both with recent oxygen isotope analyses and coupled ocean-atmosphere modelling studies, which suggest that glacial temperatures in the tropics were likely to have been intermediate between that as reconstructed by CLIMAP and suggested by corals and snow lines [Crowley, 2000; Spero *et al.*, 1997; Wolff *et al.*, 1998]. The ‘CLIMAP-2’ scenario for glacial-interglacial SST change is therefore adopted as default. The results of this are summarized in Figure 5-4. The amplitude of $x\text{CO}_2$ variability is now much greater, with a 19→0 ka BP increase of 29.6 ppmv. The associated increase in $\delta^{13}\text{C}^{\text{CO}_2}$ is similarly enhanced at some 0.33‰.

5.4.3 Wind speed driven air-sea gas transfer

Variability in the air-sea gas transfer coefficient driven by changes in wind speed has been proposed as being an important control on atmospheric composition [Erickson, 1989; Keir, 1993a], with a simple box model being able to account for around 50 ppmv of the observed deglacial increase in atmospheric CO_2 [Keir, 1993b]. As a first-order test of the potential influence of glacial-interglacial changes in surface ocean wind speeds, the LGM climate is assumed to be characterized by mean annual wind speeds 50% higher than at present. Different forcing signals are used to characterize assumed differential variability between the two hemispheres. Northern latitudes are weighted using the SPECMAP curve [Imbrie *et al.*, 1984], while southern latitudes take information regarding the timing and rates of change from the Na concentration record contained within the Vostok ice core [Petit *et al.*, 1999], a proxy for wind speeds in Southern Ocean source areas of marine aerosol production [De Angelis *et al.*, 1987; Petit *et al.*, 1981].

The results of this exercise are summarized in Figure 5-5. Differences in the nature of the response between the two hemispheres are evident; while decreasing wind speeds weighted towards NH latitudes produce a noticeable increase in $x\text{CO}_2$ (3.6 ppmv over 19→0 ka BP), SH latitudes appear to have little influence (< 0.9 ppmv over 19→0 ka BP). In contrast, it is only SH wind speeds that exert any significant

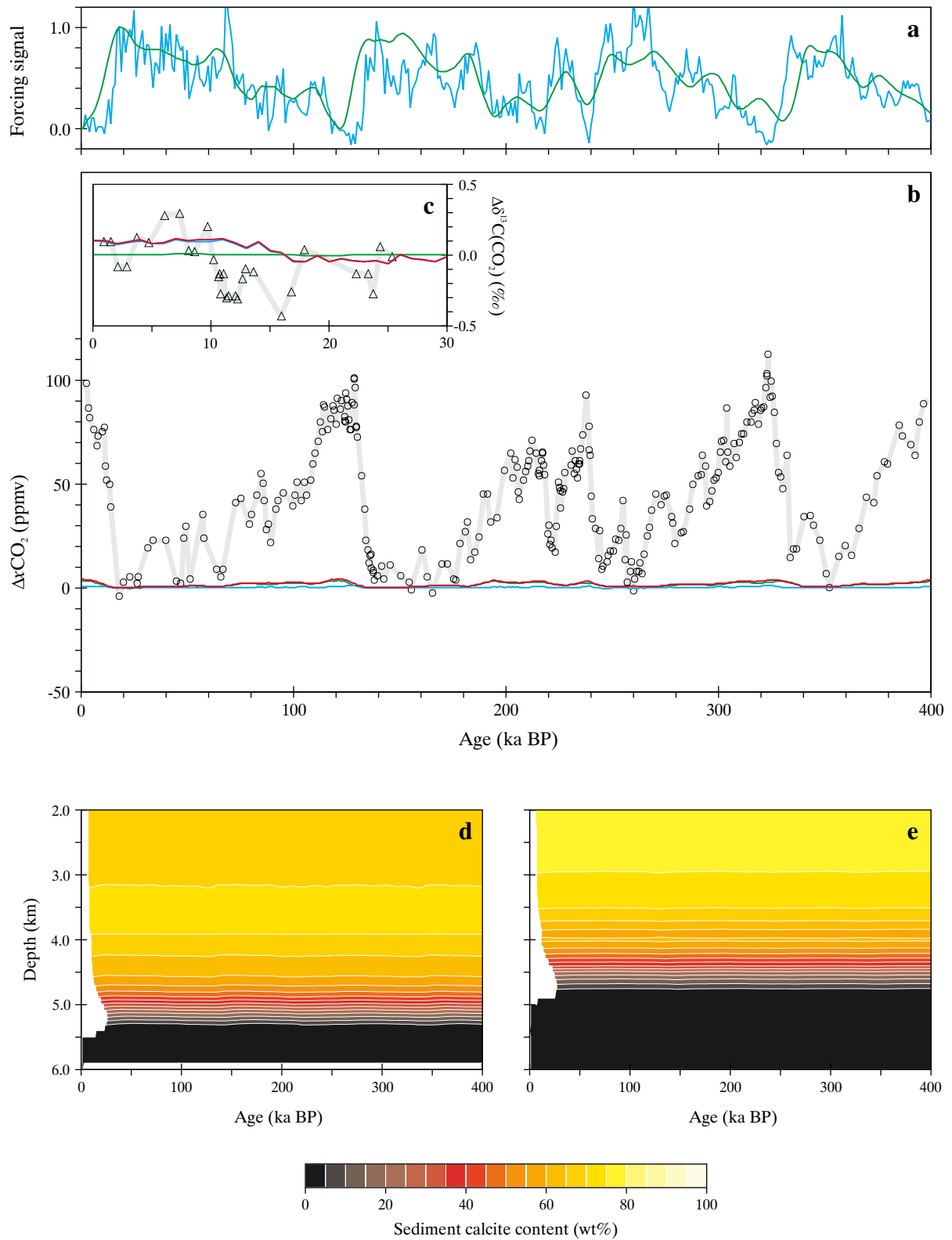


Figure 5-5 Effects on the global carbon cycle of glacial-interglacial variability in surface ocean wind speed. Shown are; (a) the NH-weighted (green) and SH-weighted (blue) forcing signals; (b) model NH-weighted (green), SH-weighted (blue) and net (red) $x\text{CO}_2$ response compared to the Vostok ice core record [Petit et al., 1999] (grey line with data points); (c) model NH-weighted (green), SH-weighted (blue) and net (red) $\delta^{13}\text{C}^{\text{CO}_2}$ response compared to the Taylor Dome ice core record [Smith et al., 1999] (grey line with data points); (d) and (e) the net response of the calcite lysocline in the (south) Atlantic and (south) Pacific basins, respectively.

control on $\delta^{13}\text{C}^{\text{CO}_2}$ – a deglacial increase of some $\sim 0.15\%$. Global reduction in wind speed consequently produces a net rise in $x\text{CO}_2$ and $\delta^{13}\text{C}^{\text{CO}_2}$ of 4.4 ppmv and 0.16% , respectively. Since only the rates of gas transfer across the air-sea interface are being modified through this test it comes as little surprise that there is virtually no detectable response in the shape and depth of the calcite lysocline (Figure 5-5d,e).

This subdued response in $x\text{CO}_2$ is at odds with previous box model results [Keir, 1993b]. One contributing factor is that a glacial enhancement in wind speed of only 50% is assumed (at the lower end of estimates derived from Antarctic ice cores [Petit *et al.*, 1981]), substantially less than the 80-150% increase considered by Keir [1993]. However, the greatest difference is probably due to the global change applied in this present study where concurrent changes in gas transfer rates in warm low latitude regions will tend to offset the influence on $x\text{CO}_2$ of changes occurring at higher colder latitudes, although both will constructively combine in terms of the net $\delta^{13}\text{C}^{\text{CO}_2}$ response. Keir [1993b] restricted changes to a single high latitude box in a class of model ocean representation strongly suspected of significantly over-estimating the effect of high latitude perturbations [Archer *et al.*, in press; Broecker *et al.*, 1999a]. The results obtained with SUE1608, with relatively little response in the atmospheric CO_2 inventory but much greater change in isotopic composition are consistent with those obtained with 3D OGCMs [Sarmiento *et al.*, 1992].

5.4.4 Sea ice extent

Reconstructions of the cryosphere at the time of the LGM suggest that seasonal sea ice cover was much more extensive than today, particularly during the summer months [CLIMAP, 1984]. A recent modelling study found that glacial-interglacial variability in Southern Ocean sea ice coverage had a profound effect on both the concentration of CO_2 in the atmosphere and on its isotopic composition [Stephens and Keeling, 2000]. To test this hypothesis, maximum (wintertime) and minimum (summertime) sea ice extent are varied, with the fractional coverage in each grid point region of the model taken from CLIMAP [1984]. Different forcing signals are used to represent the differential climatic variability characterizing the two hemispheres; northern latitudes are weighted using the SPECMAP curve [Imbrie *et al.*, 1984] while Southern latitudes take information regarding the timing and rate of change of events from the Vostok δD record [Petit *et al.*, 1999] (assuming a first-order correspondence between sea ice cover and local air temperature).

The results of this exercise are summarized in Figure 5-6. While the response of $x\text{CO}_2$ to changes in sea ice cover weighted towards either hemisphere are of a similar magnitude, the signs of glacial-interglacial change are opposite. At high northern latitudes, increased sea ice cover acts so as to effectively 'cap' what is a strong CO_2 sink region, with its deglacial retreat driving $x\text{CO}_2$ down by 11.9 ppmv over 19→0 ka BP. This can be taken as a maximum likely response, since circulation patterns in the north Atlantic

would have shifted further south during glacial periods in parallel with expanded sea ice cover. In the Southern Ocean, mean model annual surface ocean CO_2 fugacity is much more neutral with respect to atmospheric composition during interglacials such that capping this region has little direct effect. However, the overall response of the system to changes in Southern Ocean sea ice cover is more complicated than this. Increased sea ice cover suppresses biological productivity, resulting in an increased northwards advective transport of nutrients. These fuel increased export production and thus additional surface ocean CO_2 draw-down at lower latitudes, with the net effect of a deglacial reduction in sea ice cover being a 7.5 ppmv increase in $x\text{CO}_2$ over 19→0 ka. In contrast, Stephens and Keeling [2000] reported an increase of over 45 ppmv associated with a reduction of sea ice coverage of surface ocean boxes lying south of the Antarctic Polar Front (APF) in their model. Much of this inter-model contrast is probably due to the more highly idealized nature of their box model, where only 5 surface zones are resolved. A direct consequence of the lack of any representation of distinct equatorial up-welling zones (regions of intense CO_2 out-gassing in the modern ocean [Tans *et al.*, 1990]) is that only the Southern Ocean is a significant source of CO_2 to the (modern) atmosphere. The strong response of $x\text{CO}_2$ to changes in Southern Ocean sea ice cover found by Stephens and Keeling [2000] could, therefore, largely be an artefact of an initially unrealistic distribution of surface ocean $f\text{CO}_2$. Indeed, with a reduction of ice-free area by a factor of 3 in the Southern Ocean of their 'PANDORA' multi-box model, Broecker and Peng [1986] reported a reduction in $x\text{CO}_2$ of only 2 ppmv. In SUE1608, the antagonistic influences of the two hemispheres produces a relatively small net response, with a 19→0 ka BP decrease in $x\text{CO}_2$ of just 4.9 ppmv.

As with CO_2 concentrations, the response of isotopic composition is also highly hemisphere-dependent with the NH playing little role in controlling $\delta^{13}\text{C}^{\text{CO}_2}$ (a 19→0 ka BP decrease of only 0.07%). The degree of exposure of the atmosphere to the Southern Ocean has a much greater effect (primarily due to its larger surface area) with a 19→0 ka BP decrease of 0.30% , virtually identical to that reported by Broecker and Peng [1986]. The net effect of global deglacial sea ice retreat is then 0.41% . The magnitude of this change is comparable to the substantial transient excursion observed in $\delta^{13}\text{C}^{\text{CO}_2}$ at the onset of Termination I [Smith *et al.*, 1999], supporting suggestions that it is sea ice retreat that is primarily responsible for this feature [Stephens and Keeling, 2000].

The re-organization of ocean nutrient cycles driven by changes in sea ice cover results in deepening in the calcite lysoclines of ~ 400 and ~ 300 m in the Atlantic and Pacific basins, respectively (Figure 5-6d,e). Re-organization is most significant in the ocean Si cycle, with rain ratios and thus CaCO_3 dissolution distorted. Greatest CaCO_3 preservation occurs during interglacial periods when the oceanic H_4SiO_4 inventory is depleted.

Recent Southern Ocean reconstructions based upon the Modern Analogue Technique and applied to core-top and LGM diatom assemblages suggest that although the position

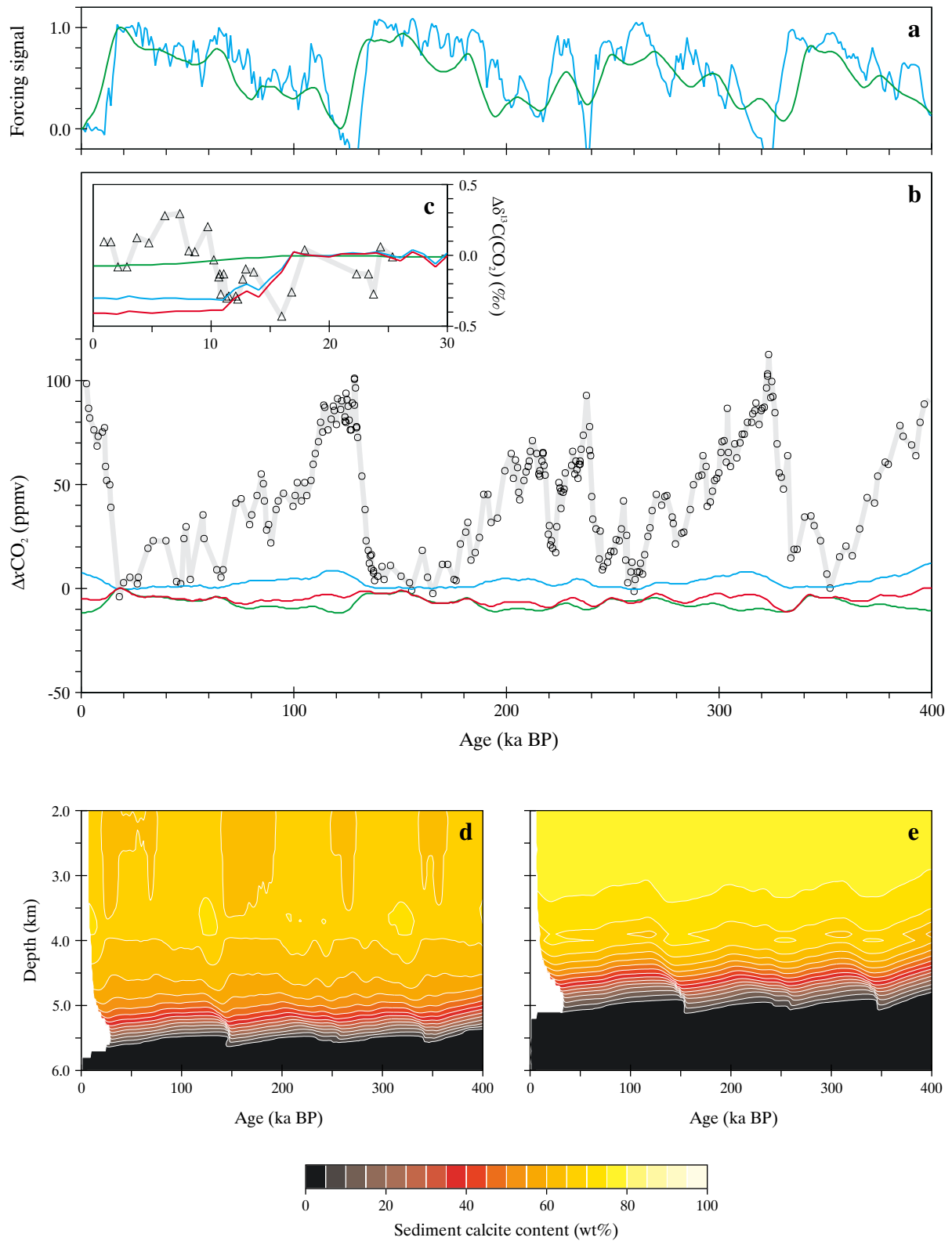


Figure 5-6 Effects on the global carbon cycle of glacial-interglacial variability in fractional sea ice cover. Shown are; (a) the NH-weighted (green) and SH-weighted (blue) forcing signals; (b) model NH-weighted (green), SH-weighted (blue) and net (red) xCO_2 response compared to the Vostok ice core record [Petit *et al.*, 1999] (grey line with data points); (c) model NH-weighted (green), SH-weighted (blue) and net (red) $\delta^{13}C^{CO_2}$ response compared to the Taylor Dome ice core record [Smith *et al.*, 1999] (grey line with data points); (d) and (e) the net response of the calcite lysocline in the (south) Atlantic and (south) Pacific basins, respectively.

of maximum (winter-time) sea ice extent was shifted much further to the north during glacial times [Crosta *et al.*, 1998a,b] in reasonable agreement with CLIMAP [1984], the position of minimum (summer-time) sea ice extent may have been little changed [Crosta *et al.*, 1998b]. The rather crude representation of sea ice extent in SUE, where a fractional coverage is applied to a zonally homogeneous ocean region, makes quantitative assessment of alternative LGM sea ice regimes difficult. Even so, summer sea ice extent appears to have a substantial effect on model $\delta^{13}\text{C}^{\text{CO}_2}$, with the assumption of constant summer sea ice extent reducing the amplitude of glacial-interglacial isotopic variability by over 50%. This sensitivity suggests that ice core records of $\delta^{13}\text{C}^{\text{CO}_2}$ could potentially help in providing additional constraints on reconstructions of past sea ice extent.

5.4.5 Ocean circulation

Changes in ocean circulation have often been invoked as a key driving force behind glacial-interglacial variations in atmospheric composition. In particular, changes in the supply of nutrients together with DIC and ALK to the surface Southern Ocean, both through variability in convective regime and advective up-welling have been suspected to produce profound changes in $x\text{CO}_2$ through the solubility and biological pumps in this region [Knox and McElroy, 1984; Martin, 1990; Sarmiento and Toggweiler, 1984]. In particular, increased surface stratification has been proposed as the single most important driver of low glacial $x\text{CO}_2$ [Francois *et al.*, 1997; Sigman *et al.*, 1999a,b]. Variations in the solubility and biological pumps arising through changes in the strength and depth of the Atlantic thermohaline circulation and through wind-driven enhancement of equatorial up-welling rates could also have played important roles [Howard and Prell, 1994; Oeschger *et al.*, 1984; Rich *et al.*, 1999; Siegenthaler and Wenk, 1984; Toggweiler, 1999].

There are few unambiguous constraints on glacial ocean circulation, particularly with respect to the details of convective and advective regimes in the Southern Ocean. This present study is also limited in scope by the requirement of a prescribed advective field. While the baseline ocean configuration of SUE1608 is derived from a modern-type ocean simulation of the Bern 2D ZOGCM [Marchal *et al.*, 1998b], there is currently no equivalent simulation available for the LGM. However, a glacial-type Atlantic circulation field is available, produced in an identical way to that for modern conditions with the exception that surface salinity in the northernmost Atlantic grid box (65°N-80°N) was restored to 34.2‰ [Marchal, pers comm]. This leads to a maximum stream function in the Atlantic, approximately half that obtained in the modern simulation and with shallower NADW, allowing increased penetration of AABW into the north Atlantic in accordance with observations [Marchal *et al.*, 1998a; Peltier and Marshall, 1995].

As a simple test of the influence of variability in Atlantic overturning circulation, the model is forced by a hybrid of modern and glacial circulations. A continuous 400 ka record is constructed assuming that the advective field at any point in time can be described as a linear combination of the two

end-member advective fields, weighted via the SPECMAP curve [Imbrie *et al.*, 1984].

The results of this exercise are summarized in Figure 5-7. There is a small 19→0 ka BP deglacial increase in $x\text{CO}_2$ of 6.3 ppmv accompanied by almost no change in $\delta^{13}\text{C}^{\text{CO}_2}$ (<0.03‰). However, altering the Atlantic thermohaline circulation produces a more substantial influence on the calcite lysocline transition zone. In the Atlantic basin, increased northwards penetration of AABW (characterized by lower carbonate ion concentrations thus being more caustic to CaCO_3) during glacial periods clearly leads to decreased CaCO_3 preservation as compared with during interglacials [Broecker *et al.*, 1993], resulting in a 600-700 m shoaling of the calcite lysocline. Ocean chemistry is balanced on a global scale through antagonistic changes occurring in the Pacific, where glacial preservation is slightly enhanced with a lysocline some ~200 m deeper. The respective sign of glacial-interglacial change in both basins is in agreement with paleoceanographic observations [Balsam, 1983; Catubig *et al.*, 1998; Farrell and Prell, 1989; Howard and Prell, 1994; Karlin *et al.*, 1992].

5.4.6 Terrestrial carbon storage

Shackleton [1977] first proposed that glacial-interglacial changes in foraminiferal $\delta^{13}\text{C}$ might indicate that transfers of carbon had occurred between the ocean (and atmosphere) and terrestrial biosphere. From measurements made on deep-sea sediment cores which suggested ambient glacial $\delta^{13}\text{C}$ conditions around 0.7‰ lighter than during the Holocene, Shackleton [1977] estimated that some 10^{18} g of carbon (1000 GtC) must have been removed from the ocean since the LGM. This was consistent with what was suspected at that time regarding a deglacial increase in carbon stored in terrestrial ecosystems through the expansion of tropical rainforests and afforestation of high northern latitudes. Should a significant quantity of carbon have been removed from the ocean and atmosphere upon deglaciation, this would effectively increase the gross deglacial CO_2 rise that other mechanisms must together explain [Berger and Wefer, 1991; Maslin, 1995]. The magnitude of the change in carbon storage is therefore of primary importance in accounting for glacial-interglacial change.

From an extensive survey of deep-sea sediment cores, Curry *et al.* [1988] concluded that an increase in mean ocean $\delta^{13}\text{C}^{\text{DIC}}$ of 0.46‰ had taken place during the last deglacial transition (19→0 ka BP), although this was subsequently reduced to 0.32‰ [Duplessy *et al.*, 1988]. Further re-analysis of benthic $\delta^{13}\text{C}$ data now suggests a mean oceanic $\delta^{13}\text{C}$ increase intermediate between the two, perhaps ~0.40‰ [Crowley, 1995]. To translate this into an equivalent shift in terrestrial biospheric carbon requires an estimate to be made of the mean isotopic composition of terrestrial organic carbon. This lies in the range -22 to -25‰ for the pre-industrial biosphere [Bird *et al.*, 1994]. However, the mean isotopic composition of land biota cannot be guaranteed to have remained invariant over the course of the late Quaternary, with a shift in the dominance of C_4 over C_3 species suspected to have occurred since the LGM [Crowley,

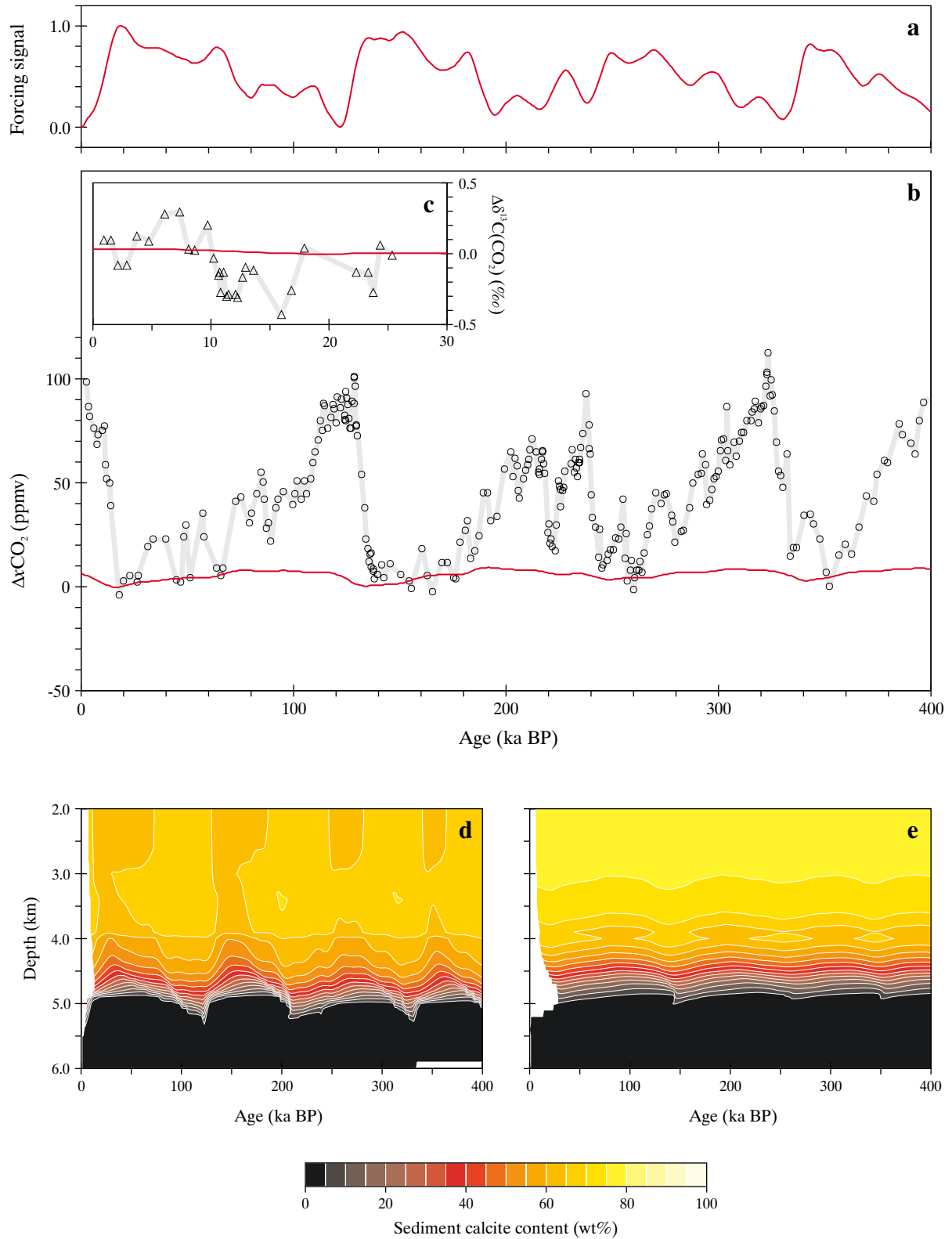


Figure 5-7 Effects on the global carbon cycle of glacial-interglacial variability in Atlantic overturning circulation. Shown are; (a) the forcing signal (normalized to a value of unity at the LGM); (b) model $x\text{CO}_2$ response (red line) compared to the Vostok ice core record [Petit *et al.*, 1999] (grey line with data points); (c) model $\delta^{13}\text{C}^{\text{CO}_2}$ response (red line) compared to the Taylor Dome ice core record [Smith *et al.*, 1999] (grey line with data points); (d) and (e) the response of the calcite lysocline in the (south) Atlantic and (south) Pacific basins, respectively.

1991, 1995; Maslin *et al.*, 1995]. Further complications arise as a result of recent culture studies, which have found a dependence on ambient carbonate ion concentrations ($[\text{CO}_3^{2-}]$) of the degree of calcitic ^{13}C fractionation in several planktonic foraminiferal species [Spero *et al.*, 1997]. If benthic species were to behave in a comparable manner then changes in deep sea $[\text{CO}_3^{2-}]$ might act to either amplify or diminish apparent variations in $\delta^{13}\text{C}^{\text{DIC}}$ recorded by foraminiferal tests [Russell and Spero, 2000]. Changes in foraminiferal $\delta^{13}\text{C}$ would therefore need to be interpreted in light of glacial-interglacial perturbations in oceanic DIC and ALK inventories, both of which are poorly constrained.

There are independent methods available for quantifying the deglacial change in carbon stored in the terrestrial biosphere, primarily through the reconstruction of terrestrial ecosystems (and their associated soils) both for LGM and modern (pre-industrial) conditions. This can be done either directly from terrestrial proxy evidence [Adams *et al.*, 1990; Adams and Faure, 1998; Crowley, 1995; Faure *et al.*, 1996; Maslin *et al.*, 1995] or by means of climate-vegetation models [Esser and Lautenschlager, 1994; Francois *et al.*, 1998, 1999; Friedlingstein *et al.*, 1992; Peng *et al.*, 1998; Prentice and Fung, 1990; Van Campo *et al.*, 1993]. Estimates made by these two methods often do not entirely agree, however, either amongst themselves or when compared with estimates based on oceanic $\delta^{13}\text{C}^{\text{DIC}}$ changes [Bird *et al.*, 1994; Crowley, 1991, 1995; Maslin *et al.*, 1995] as summarized in Table 5-3. That reconstructions suggest increases ranging from -100 GtC to 1900 GtC puts a high degree of uncertainty on the

Table 5-3 Estimates of the Increase in Carbon Stored in Terrestrial Ecosystems Since the LGM (ΔC)

ΔC (GtC)	Reference
foraminiferal $\delta^{13}\text{C}$ changes	
700	Curry <i>et al.</i> [1988]
490	Duplessy <i>et al.</i> [1988]
1070	Shackleton [1977]
610	Crowley [1995]
paleovegetation reconstructions	
1351	Adams <i>et al.</i> [1990], Faure <i>et al.</i> [1996]
900 to 1900	Adams and Faure [1998]
1100	Maslin <i>et al.</i> [1995]
760 to 1040	Crowley [1995]
coupled climate-vegetation models	
134 ¹ to 606	Francois <i>et al.</i> [1998]
-460 ¹ to 213	Esser and Lautenschlager [1994]
-70 to 710	Francois <i>et al.</i> [1999]
-30	Prentice and Fung [1990]
300	Friedlingstein <i>et al.</i> [1992]

¹ Assuming no CO_2 fertilization effect on net primary productivity

importance to observed glacial-interglacial variability in atmospheric composition of the transfer of carbon between the terrestrial biosphere and ocean and atmosphere.

The perturbing effect that changes in terrestrial vegetation might have had on the global carbon cycle is now investigated by varying the magnitude of the terrestrial carbon reservoir. As an initial test, 500 GtC is assumed to have been removed from the atmosphere following the LGM; a value chosen to be consistent with the mid-point of the range of estimates made from observed foraminiferal $\delta^{13}\text{C}$ change and climate-vegetation models. The SPECMAP $\delta^{18}\text{O}$ stack [Imbrie *et al.*, 1984] is taken as a first-order proxy for glacial-interglacial variability in the terrestrial reservoir.

The results of this exercise are summarized in Figure 5-8. It can be seen that the effect of an expansion of the terrestrial biosphere is to reduce $x\text{CO}_2$ by a total of 24.7 ppmv for the interval 19→0 ka BP, contrary to the sign of the observed change. The magnitude of this decrease is greater than suggested by other models that predict change in the range 12 to 17 ppmv [Archer *et al.*, 2000; Broecker and Peng, 1986]. However, these all assume that a steady state with respect to deep-sea CaCO_3 has been reached (i.e., through 'carbonate compensation'). This process occurs with an e -folding time of ~9 ka such that if the main transfer of carbon were to be centred around ~10 ka BP then the reduction in oceanic DIC inventory will be far from having been fully compensated for. Indeed, Archer *et al.* [2000] reported that the uncompensated change in $x\text{CO}_2$ in response to a 500 GtC perturbation is almost 40 ppmv. Thus not only is the absolute magnitude of the change in terrestrial carbon storage of fundamental importance to the response of the system but so too is the rate of this change. Associated with the deglacial reduction in $x\text{CO}_2$ is a gradual increase in $\delta^{13}\text{C}^{\text{CO}_2}$ of ~0.31‰.

The response of the calcite lysocline in both the Atlantic and Pacific basins is very similar, with weak preservational spikes characterized by a 200-300 m deepening, synchronous with the deglacial transitions. These transients of enhanced preservation are slightly greater in depth for the aragonite lysocline (not shown) than for calcite, and are consistent with observations of CaCO_3 preservation between the end of the LGM and early Holocene [Berger, 1977; Broecker *et al.*, 1993, 1999b].

5.4.7 Neritic sediment storage

A number of hypotheses to explain glacial-interglacial variations in atmospheric CO_2 concentrations have been based upon the extraction from the ocean (during interglacial periods of high sea level) and temporary storage in continental shelf sediments of materials whose presence would otherwise tend to exert a negative pressure on $x\text{CO}_2$. The earliest of such schemes was the 'Phosphate Extraction Model', in which the removal of organic phosphate from the ocean resulted in the limiting of ocean productivity and thus higher $x\text{CO}_2$. During glacial times, PO_4 returned to the ocean through shelf sediment erosion fuels ocean productivity, leading to lower $x\text{CO}_2$ [Broecker, 1982; Broecker and Peng, 1982]. However, as a sole explanation for the magnitude of

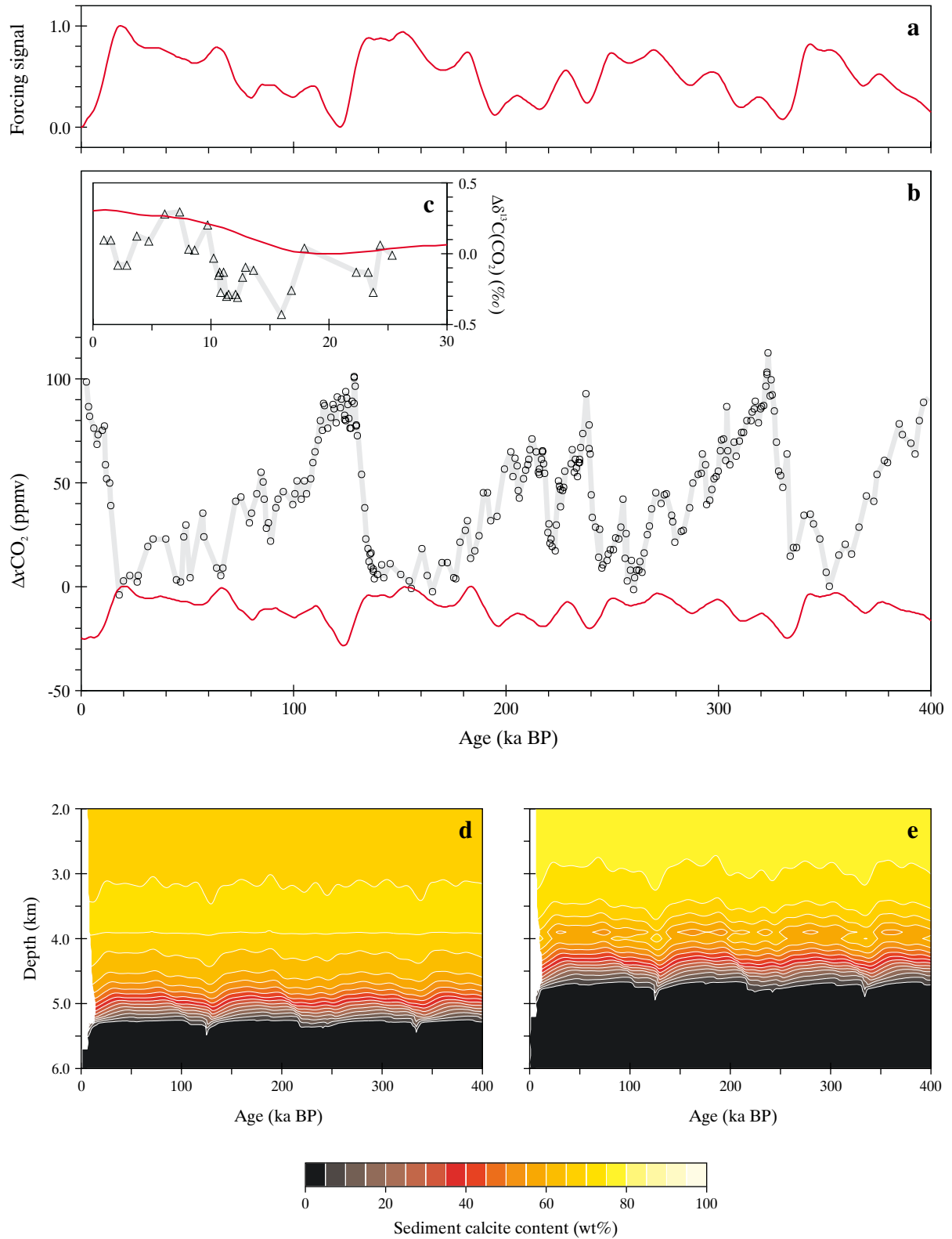


Figure 5-8 Effects on the global carbon cycle of glacial-interglacial variability in terrestrial carbon storage. Shown are; (a) the forcing signal (normalized to a value of unity at the LGM); (b) model $x\text{CO}_2$ response (red line) compared to the Vostok ice core record [Petit et al., 1999] (grey line with data points); (c) model $\delta^{13}\text{C}^{\text{CO}_2}$ response (red line) compared to the Taylor Dome ice core record [Smith et al., 1999] (grey line with data points); (d) and (e) the response of the calcite lysocline in the (south) Atlantic and (south) Pacific basins, respectively.

glacial-interglacial change it fell foul of considerations such as observed changes in oceanic $\delta^{13}\text{C}$ [Keir and Berger, 1983; Knox and McElroy, 1984], Cd/Ca ratios [Boyle, 1988; Shaffer, 1990], dissolved oxygen concentrations [Knox and McElroy, 1984], and the tendency for $x\text{CO}_2$ rise to lag sea level change contrary to the observed sequence of events surrounding glacial terminations [Barnola et al., 1987; Sowers et al., 1991].

5.4.7.1 The 'Coral Reef Hypothesis'

A variant on the phosphate extraction model that avoids many of the above-mentioned proxy violations considers the deposition of CaCO_3 in shelf sediments. This envisages that glacial-interglacial changes in the rate of accumulation of CaCO_3 in the neritic environment driven by sea level change would perturb global ocean chemistry and thus atmospheric composition [Berger, 1982a,b; Keir and Berger, 1983, 1985; Opdyke and Walker, 1992]. This is known as the 'Coral Reef Hypothesis' [Berger, 1982a], although accumulation of CaCO_3 can take place as both reefal (coral-derived) and non-reefal (unconsolidated sediments) components. Simple logic supports the notion that there must have been a significant degree of variability in CaCO_3 accumulation rates over the late Quaternary; reduced submerged continental shelf area during glacial periods would result in a lower global rate of CaCO_3 accumulation compared to interglacials. Indeed, erosion of carbonate-rich sediments from exposed shelves may even have produced a net transfer of CaCO_3 back during times of low sea level stand. Although deep-sea sediments will eventually counteract any perturbation in the magnitude of shelf accumulation rates via transient changes in the depth of the lysocline, this only occurs with an e -folding time of the order of 10 ka. Changes in sea level (and thus neritic accumulation rates) will therefore produce a degree of disequilibrium between benthic sediments and ocean chemistry. It is this disequilibrium that allows the oceanic inventories of DIC and ALK to be perturbed, affecting $x\text{CO}_2$ [Berger, 1982b]. As with the phosphate extraction model, such atmospheric changes will, at best, lag sea level change, invalidating the coral reef hypothesis as a sole explanation for the observed deglacial $x\text{CO}_2$ rise [Broecker and Henderson, 1998]. However, it might play an important role in the later part of the deglacial transition, for instance in counteracting the downward forcing pressure upon $x\text{CO}_2$ due to the buildup of carbon in the terrestrial biosphere (5.4.6) [Berger, 1982b; Broecker and Peng, 1993; Maslin et al., 1995].

Accurate estimation of the magnitude of glacial-interglacial change in neritic CaCO_3 accumulation is far from straightforward. Areal accumulation rates have previously been derived from estimates made of neritic CaCO_3 build-up over the course of the late Holocene [Mundhoven and Francois, 1996; Walker and Opdyke, 1995], taken to be 7×10^{12} and 7.5×10^{12} mol $\text{CaCO}_3 \text{ a}^{-1}$, for reefal and non-reefal components, respectively [Milliman, 1993]. For reefal accumulation this figure is independently corroborated by process-based global models of coral reef growth [Kleypas, 1997]. Erosion rates are especially hard to quantify, with values previously either adapted from observed terrestrial weathering rates [Mundhoven and Francois, 1996] or simply

treated as a model tuning parameter [Opdyke and Walker, 1992]. As an initial test of the potential role of this mechanism, the parameterization of Mundhoven and Francois [1996] is adopted. Sea level history is the same as assumed previously (5.4.1).

The results of this exercise are summarized in Figure 5-9. It can be seen that the coral reef hypothesis as formulated by Mundhoven and Francois [1996] has a very substantial influence on $x\text{CO}_2$, with a total 19→0 ka BP increase of 45.9 ppmv. This is despite the concurrent effect of sea level change alone (i.e., excluding SSS changes) being some 7.7 ppmv in the opposite direction. Changes in the oceanic inventory of DIC and ALK in the ocean therefore drive a total deglacial increase of 53.6 ppmv, almost two thirds of the observed increase [Petit et al., 1999] and consistent with comparable models [Mundhoven and Francois, 1994, 1996; Opdyke and Walker, 1992; Walker and Opdyke, 1996]. There is virtually no associated change in atmospheric $\delta^{13}\text{C}^{\text{CO}_2}$ (<0.02‰).

Although this appears to offer a simple means of explaining much of the observed amplitude of glacial-interglacial change in $x\text{CO}_2$ there appears to be a serious problem with the magnitude of the perturbation in deep-sea sediments which it drives (Figure 5-9d,e). Both basins exhibit glacial deepening in the depth of the calcite lysocline of between 1 and 2 km. Changes of this order in the Pacific are not supported by available data [Berger, 1978, 1982b; Farrell and Prell, 1989, 1991; Karin et al., 1992]. Furthermore, observed Atlantic changes are opposite in sign to that predicted by the model [Balsam, 1983; Berger, 1968; Crowley, 1983; Gardner, 1975]. It is unlikely that additional mechanisms might act so as to correct excess CaCO_3 preservation of this degree. Either the magnitude of changes in neritic CaCO_3 storage must have then been over-estimated, or deficiencies in the model CaCO_3 cycle artificially magnify the response of the system. In the latter case, the apparent under-estimation of CaCO_3 content in the equatorial zones of the ocean as well as in several mid-latitude regions (4.4.3) might reduce the overall buffering capacity of the deep-sea sediment system with respect to changes in neritic CaCO_3 accumulation rates. Variability in CaCO_3 preservation in other regions of the world ocean (coincidentally the locations the synthetic sediments cores used for reconstructing the two lysocline sections) would thus be intensified.

A more plausible response of the CaCO_3 lysocline can be obtained by reducing the rate of neritic build-up and erosion (both reefal and non-reefal components) by 50%. This results in a maximum glacial-interglacial difference in deposition rates of $\sim 7 \times 10^{12}$ mol $\text{CaCO}_3 \text{ a}^{-1}$. To re-balance ocean DIC and ALK inventories over the long term, the influence of CaCO_3 dissolution through the oxidation of organic carbon within the sediments (3.2.4) is reduced by 50%, thereby increasing deep-sea CaCO_3 preservation and making up the neritic shortfall. This has the desirable side-effect of generally improving the global distribution of CaCO_3 -rich sediments in the model (not shown), with sedimentary CaCO_3 distributions much closer to

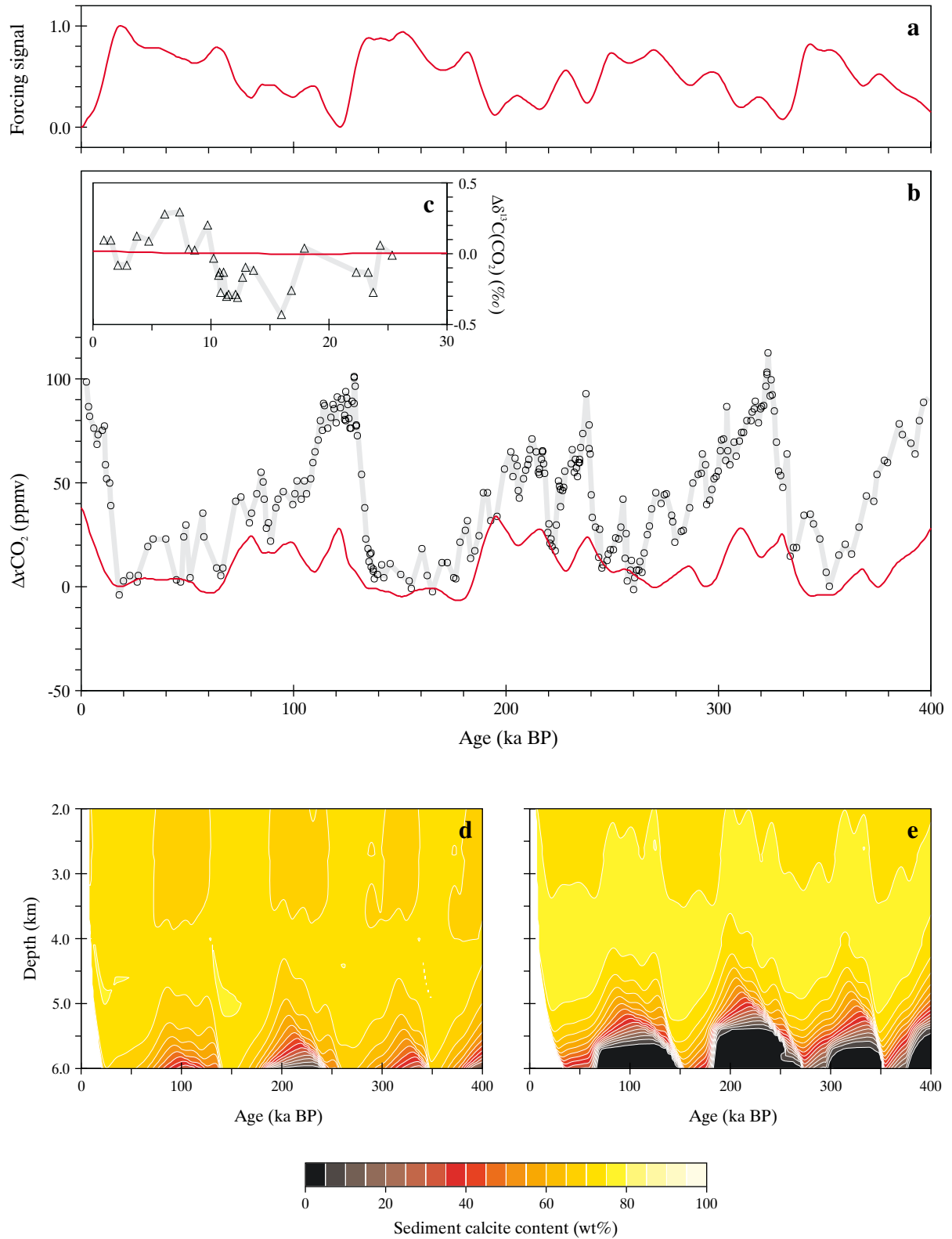


Figure 5-9 Effects on the global carbon cycle of glacial-interglacial variability in neritic CaCO₃ storage. Shown are; (a) the forcing signal (normalized to a value of unity at the LGM); (b) model $\Delta x\text{CO}_2$ response (red line) compared to the Vostok ice core record [Petit et al., 1999] (grey line with data points); (c) model $\delta^{13}\text{C}^{\text{CO}_2}$ response (red line) compared to the Taylor Dome ice core record [Smith et al., 1999] (grey line with data points); (d) and (e) the response of the calcite lysocline in the (south) Atlantic and (south) Pacific basins, respectively.

observations in the equatorial Atlantic and Pacific zones and in the Indian Ocean.

The peak-to-peak amplitude in $x\text{CO}_2$ variability is now almost exactly 50% of that obtained before, with a rise of 22.5 ppmv over the interval 19→0 ka BP. Importantly, changes in lysocline depth are much more modest. While Atlantic change is still in a direction opposite to that observed, it is no longer overwhelmingly so (~900 m). A glacial-interglacial amplitude of 400-600 m in the Pacific is consistent with observations.

5.4.7.2 Introducing the 'Opal Extraction Model'

An analogue to the phosphate extraction model can be found in the limiting nutrient silicic acid, with variable accumulation rates of biogenic opal deposited on continental shelves in response to changes in sea level likely. Indeed, the potential significance of this mechanism to the global carbon cycle is highlighted by estimates made of the present-day ocean sink of H_4SiO_4 in neritic sediments equivalent to ~20% of the entire abyssal ocean sink ($5.9 \text{ Tmol Si a}^{-1}$) [Treguer *et al.*, 1995]. While the effect of glacial-interglacial variability in H_4SiO_4 may not significantly alter the absolute strength of the biological pump, the favouring of siliceous phytoplankton over non-siliceous species will alter the CaCO_3 :POC rain ratio, driving changes in ocean chemistry and thus $x\text{CO}_2$ [Archer and Maier-Reimer, 1994; Harrison, 2000].

To test this hypothesis, a simple model is constructed based directly upon the neritic (non-reefal component) CaCO_3 sediment accumulation model of Mundhovan and Francoise [1996]. Specific opal accumulation rates are chosen to reproduce estimated mean global neritic buildup during the late Holocene ($1.2 \text{ Tmol Si a}^{-1}$) [Treguer *et al.*, 1995]. Since little is known regarding possible rates of erosion of previously-deposited material, no erosional term is included. A variable oceanic sink for H_4SiO_4 of between 0.36 and $1.21 \text{ Tmol Si a}^{-1}$ thus arises as a function of sea level.

The action of this mechanism is to produce a small deglacial (19→0 ka BP) decrease in $x\text{CO}_2$ of 5.4 ppmv with virtually no associated effect on $\delta^{13}\text{C}^{\text{CO}_2}$. These results, together with the interglacial shoaling of the calcite lysocline (some ~300 m in the Atlantic basin), are practically indistinguishable from the effects of sea level change alone, suggesting that this mechanism has little influence on the global carbon cycle (at least in isolation).

5.4.8 Dissolved silica supply to the ocean

Interest has recently been stimulated in the role that changes in the dissolved Si input to the ocean may have had on glacial-interglacial $x\text{CO}_2$ variability. This has arisen out of the potential for the ocean Si cycle, with a residence time for dissolved Si of ~15 ka, to account for the lag of up to 8 ka that occurs between the start of dust decline towards the end of Stages 2 and 6, and the initial CO_2 rise that follows in each core [Broecker and Henderson, 1998]. On this basis, Harrison [2000] proposed a 'Silica Hypothesis', whereby increased glacial aeolian Si supply to the surface ocean enhances diatom productivity at the expense of calcium carbonate

shell-forming species, thus affecting $x\text{CO}_2$ via the 'rain ratio hypothesis' [Archer and Maier-Reimer, 1994]. Harrison [2000] went further to suggest the entire glacial-interglacial $x\text{CO}_2$ difference might be explained in this way. Increases in dissolved Si supply to the oceans driven by changes in the weathering rate of continental (silicate) rock might further enhance this effect [Treguer and Pondaven, 2000]. The potential role of these mechanisms in perturbing the global carbon cycle are now individually assessed.

5.4.8.1 Aeolian flux

To test the hypothesis that glacial-interglacial changes in dissolved Si supply derived from aeolian silicates exert a strong control over atmospheric CO_2 levels, dust deposition to the surface ocean is varied. Modern dust deposition to the model ocean surface is some $6.85 \times 10^{14} \text{ g a}^{-1}$ [Mahowald *et al.*, 1999]. Assuming that SiO_2 comprises 66 wt% of dust (mean upper continental crustal abundance [Taylor and McLennan, 1985]) gives a solid input of some $4.52 \times 10^{14} \text{ g SiO}_2 \text{ a}^{-1}$, equivalent to $7.54 \text{ Tmol Si a}^{-1}$. To achieve a value for total aeolian dissolved Si input $0.5 \text{ Tmol Si a}^{-1}$ consistent with Treguer *et al.* [1995] therefore requires a solubility of ~6.6%, in line with experimental estimates [Wollast and Chou, 1985]. Dissolved (riverine) Si supply is reduced by an equivalent amount in the model in order to balance the (modern) ocean budget. For the LGM, the equivalent global dust deposition flux is $2.29 \times 10^{14} \text{ g a}^{-1}$ [Mahowald *et al.*, 1999] giving a peak glacial aeolian dissolved Si flux of $1.67 \text{ Tmol Si a}^{-1}$, more than 3 times greater than at present. The temporal variability in the Vostok dust concentration record [Petit *et al.*, 1999] is used as a proxy for relative changes in global dust deposition fluxes in order to reconstruct a record for the last 400 ka. Aeolian iron supply is held constant for the purpose of this experiment.

The results of this exercise are summarized in Figure 5-10. It can be seen that there is a rather minimal response in $x\text{CO}_2$ to this forcing with a glacial-interglacial amplitude of less than 2.2 ppmv and virtually no detectable change in $\delta^{13}\text{C}^{\text{CO}_2}$. Similarly, sedimentary CaCO_3 contents in both Atlantic and Pacific basins are little affected. Sensitivity analyses suggest that even by assuming a solubility for aeolian SiO_2 as high as 14.2% (sufficient to produce a 50% increase in total dissolved Si supply at the LGM over present-day rates) the 19→0 ka BP deglacial increase in $x\text{CO}_2$ is proportionally increased only to ~6 ppmv.

5.4.8.2 Riverine fluxes

To test the secondary hypothesis, that glacial-interglacial changes in riverine dissolved Si supply might have produced a significant effect on $x\text{CO}_2$, the riverine input to the ocean is varied. Glacial rates of supply were set some $1.0 \text{ Tmol Si a}^{-1}$ higher than at present, comparable in peak amplitude to the aeolian experiment (5.4.8.1). However, the SPECMAP $\delta^{18}\text{O}$ stack [Imbrie *et al.*, 1984] is now used as a proxy for relative changes in weathering-derived fluxes in order to reconstruct a forcing record for the last 400 ka.

As with aeolian Si supply, the response of atmospheric composition to the forcing is small, with a 19→0 ka BP increase in $x\text{CO}_2$ of 2.4 ppmv and no detectable change in

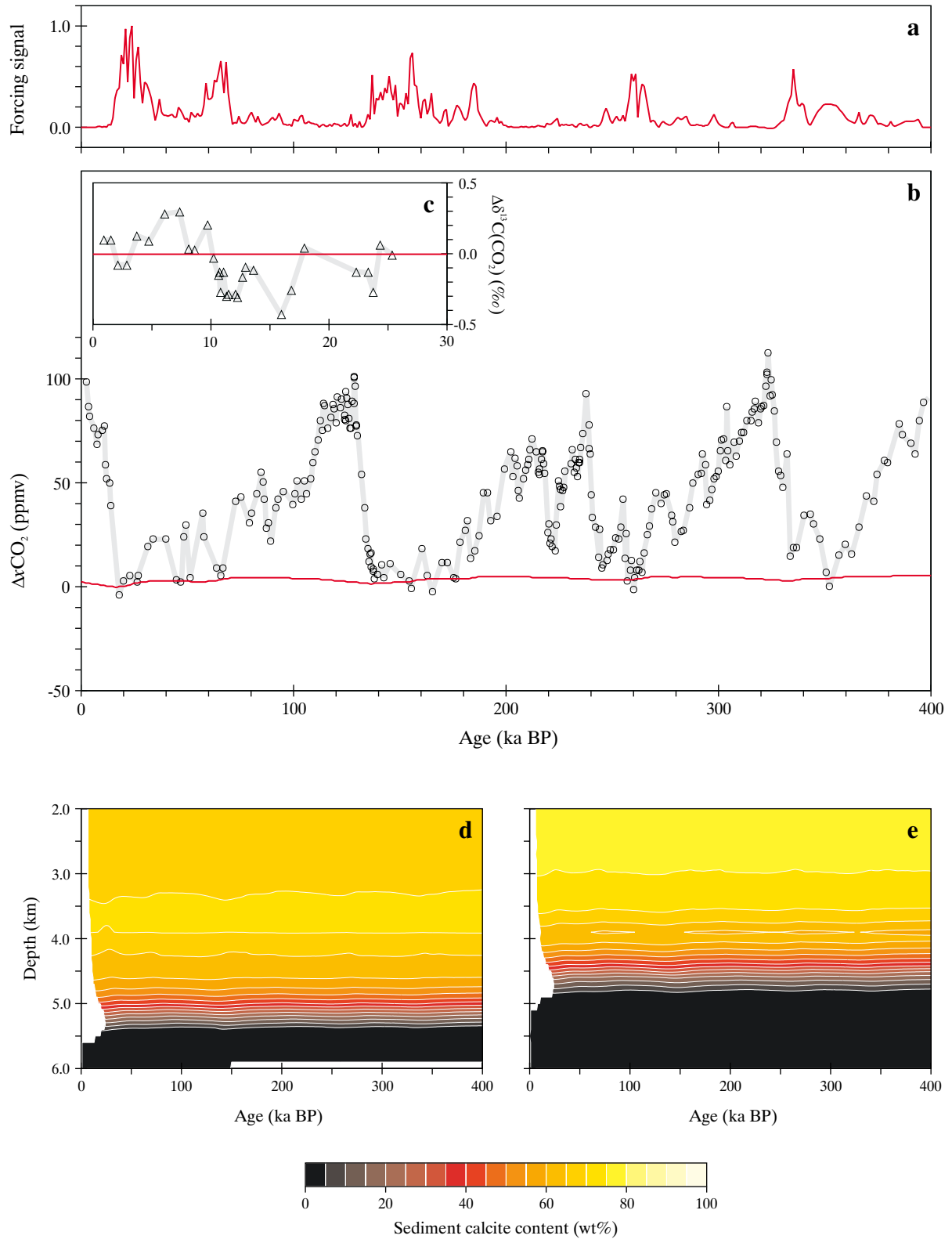


Figure 5-10 Effects on the global carbon cycle of glacial-interglacial variability in aeolian Si supply. Shown are; (a) the forcing signal (normalized to a value of unity at the LGM); (b) model $x\text{CO}_2$ response (red line) compared to the Vostok ice core record [Petit et al., 1999] (grey line with data points); (c) model $\delta^{13}\text{C}^{\text{CO}_2}$ response (red line) compared to the Taylor Dome ice core record [Smith et al., 1999] (grey line with data points); (d) and (e) the response of the calcite lysocline in the (south) Atlantic and (south) Pacific basins, respectively.

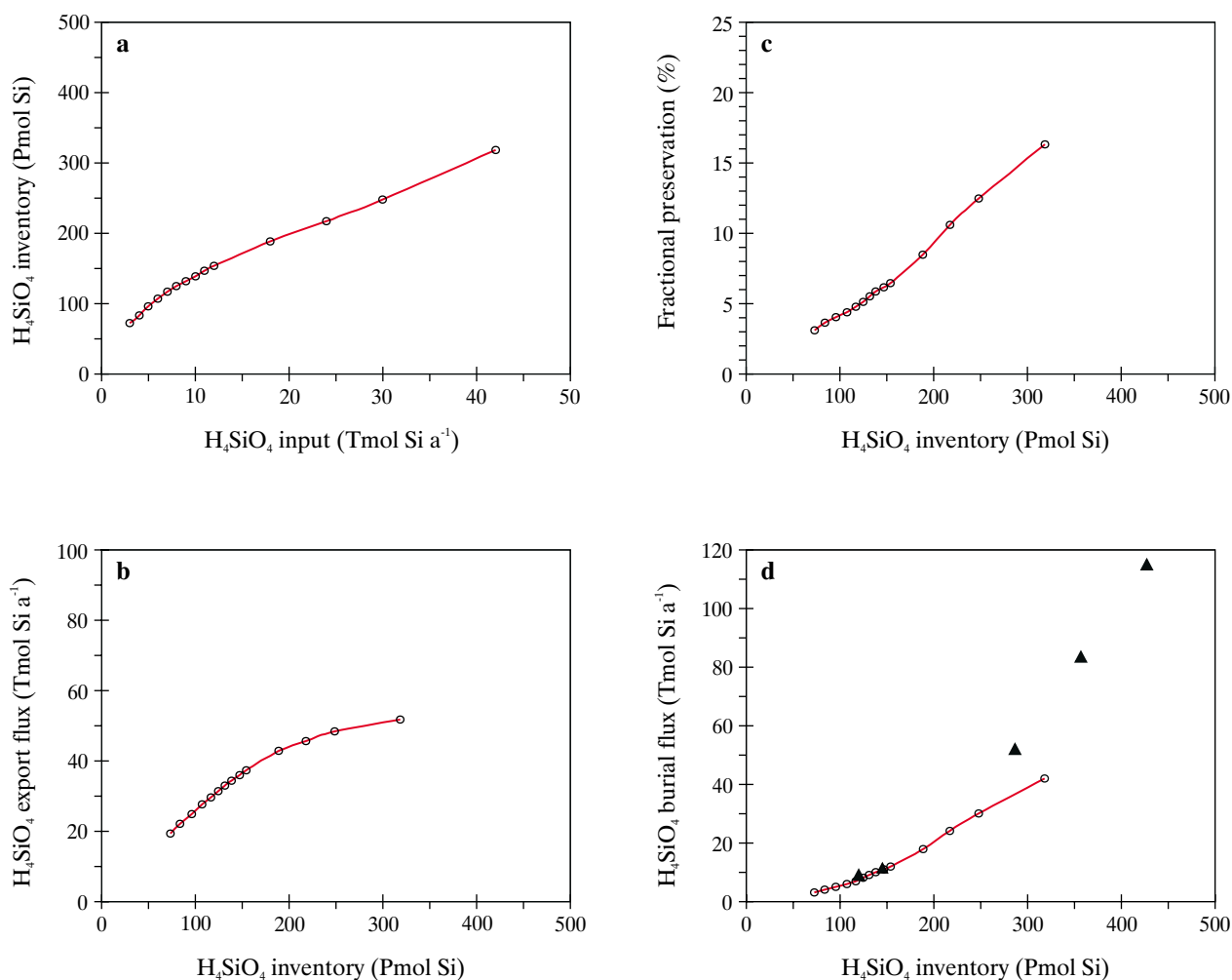


Figure 5-11 Relationships within the ocean Si cycle in response to changing dissolved Si supply.

$\delta^{13}C^{CO_2}$. Despite substantial differences in the shape and integrated area of the forcing signal used for weathering rate change compared to that in the aeolian deposition experiment, the overall effect on the global carbon cycle is similar. There is slightly greater variability in the depth of the calcite lysocline, although a glacial shoaling of ~ 100 m is still relatively minor. Sensitivity analyses again suggest that enhancing the strength of the forcing produces a proportional (but still small) atmospheric response.

5.4.8.3 Oceanic Si cycling and the ‘Silica Hypothesis’

Contrary to conceptual schemes purporting to explain glacial-interglacial change in atmospheric composition via increased dissolved Si supply to the world ocean during glacial times [Harrison, 2000; Treguer and Pondaven, 2000], the results of a mechanistic ocean silica cycle model suggest that there is little effect. This present study supports the conclusions of Archer *et al.* [2000] that attempting to change the oceanic inventory of H_4SiO_4 is a relatively ineffective way

of altering xCO_2 . However, it is an interesting question as to what processes operating within the system are responsible for the surprisingly damped response to what appear quite substantial perturbations in the supply of this key nutrient.

One contributing factor relates to the time-varying nature of the perturbations employed in this study. Some of the more prominent features in the Vostok dust concentration [Petit *et al.*, 1999] and SPECMAP $\delta^{18}O$ [Imbrie *et al.*, 1984] forcing signals (such as deglacial transitions) are characterized by time scales of only 2-5 ka. This is short compared to the residence time of H_4SiO_4 in the ocean which in SUE1608 is about 16 ka (consistent with estimates of 10-20 ka derived from modelling and mass balance considerations [Archer *et al.*, 2000; Treguer *et al.*, 1995]). Furthermore, when interactions between $CaCO_3$ and silica cycles within the carbon cycle as a whole are taken into account, the e -folding time of changes in atmospheric composition with respect to perturbations in dissolved Si supply is even longer, some ~ 23 ka. Variability in the xCO_2

response to changes in dissolved Si input are therefore highly damped. This is in contrast to that expected by *Harrison* [2000] and *Treguer and Pondaven* [2000] who implicitly assume a system at steady-state.

An equally important contributor to overall system response involves the dynamics of Si burial, with *Archer et al.* [2000] finding that since Si burial appeared to rise with the second power of H_4SiO_4 inventory it would be extremely difficult to significantly change the H_4SiO_4 inventory through increased Si supply in the first place. Results of sensitivity analyses carried out with SUE1608 and driven by (total) dissolved Si inputs to the ocean of between 3 and 42 Tmol Si a^{-1} are shown in Figure 5-11. For this test, following a spin-up period, a step increase in dissolved Si input is applied and the system allowed to adjust for a further 50 ka (thus achieving ~95% of true steady state). The resulting model state is then compared to a control run forced continuously with the baseline dissolved Si input (6 Tmol Si a^{-1}). From this it can be seen that the oceanic H_4SiO_4 inventory is relatively insensitive to the dissolved Si input; a 14-fold increase in input is required to produce just over a 4-fold increase in inventory (Figure 5-11a). Export production of biogenic opal appears to be linear with H_4SiO_4 inventory over a range spanning plausible dissolved Si input rates to the ocean (3-12 Tmol Si a^{-1}) above which there is a rapid decline in slope with further increases in H_4SiO_4 availability (probably due to a maximum shift in species composition towards siliceous phytoplankton having been approached). These effects, together with a scaling of sedimentary opal preservation efficiency with H_4SiO_4 inventory (Figure 5-11c) combine to produce a non-linear response of burial flux with H_4SiO_4 inventory (Figure 5-11d). This final relationship is consistent with results from 3D OGCM carbon cycle modelling work suggesting an approximately parabolic relationship [*Archer et al.*, 2000]. However, in SUE1608 this relationship breaks down at an inventory of around 225 Pmol Si as a result of the saturation in export flux (Figure 5-11b).

The apparent failure of the 'Silica Hypothesis' in the model employed here can now be assessed in light of these two factors. In order to explain low glacial levels of CO_2 an increase in the oceanic H_4SiO_4 inventory of between about 10% and 67% (depending upon assumptions made regarding ecosystem composition and interaction) was suggested to be sufficient [*Harrison*, 2000]. Taking the absolute minimum requirement, a 10% increase in H_4SiO_4 inventory requires a 32% increase in dissolved Si input (Figure 5-11a), equivalent to an additional ~1.9 Tmol Si a^{-1} . This could be achieved with a solubility for aeolian silicates of about 11%, higher than available estimates allow for [*Wollast and Chou*, 1985] (but not unreasonably so). Given that the full width at half maximum (FWHM) of the Stage 2 dust peak in the Vostok core is only of order 10 ka, the 16 ka oceanic Si residence time suggests that solubility would have to be substantially greater in order to have attained the required increase in H_4SiO_4 inventory by the end of the LGM. Indeed, a peak aeolian influx of over 4.4 Tmol Si a^{-1} corresponding to a solubility of SiO_2 of ~25% is required in SUE1608 to produce such an inventory. Solubilities of this order are highly unlikely. A further problem with this hypothesis

concerns the uniform global distribution assumed of phytoplankton species abundance and thus of export ratio [*Harrison*, 2000]. With the exception of equatorial up-welling regions, most deep-sea sediment CaCO_3 accumulation tends to occur beneath regions where diatoms are responsible for a relatively minor proportion of POC export. In such regimes, a 10% increase in the POC export from siliceous species would result in much less than a 10% decrease in non-siliceous POC export and thus less than a 10% decline in CaCO_3 flux. The minimum increase needed in H_4SiO_4 inventory to achieve the required reduction in CaCO_3 export by *Harrison* [2000] would therefore be greater, further adding to the aeolian SiO_2 solubility requirement.

By similar arguments, the solubility requirement of an ocean nutrient cycle model [*Tyrrell*, 1999] used in the variation of the hypothesis put forward by *Treguer and Pondaven* [2000] proves to be even worse. In this, model glacial $x\text{CO}_2$ levels are explained by a 48% increase in biogenic opal export. If a similar increase in H_4SiO_4 inventory is required as an absolute minimum, an additional dissolved Si input of 6.6 Tmol Si a^{-1} is needed at steady state. The solubility requirement is now already 16% – this is before either the transitory nature of the input forcing or spatial heterogeneity in species composition have been taken into account.

Additional model experiments suggest that even a combination of aeolian supply and riverine influx fall far short of being able to account for the magnitude of observed $x\text{CO}_2$ changes. Indeed, with an assumption of 10% aeolian SiO_2 solubility together with a 50% LGM enhancement in riverine input, $x\text{CO}_2$ increases by only ~9 ppmv (19→0 ka BP). The response time of the system with respect to changes in dissolved supply is too long for any significant role to be played in the initial observed rapid rise in atmospheric CO_2 levels, with just ~2 ppmv occurring before Termination I is substantially complete by 10 ka BP. Despite this, changes in the global Si cycle may yet be important in driving declining $x\text{CO}_2$ as glaciations deepen, being responsible in this test for as much as 18 ppmv of the overall trend apparent between Stages 5a and 2.

5.4.9 The 'Iron Hypothesis'

One of the great puzzles in oceanography has been the reason for the existence of certain areas of the world ocean, particularly the Southern Ocean together with the equatorial and north Pacific, where there is an abundance of unused macro-nutrients [*de Baar and Boyd*, 2000]. Although physical (solar insolation and ocean surface mixing) and grazing regimes must play a part in controlling phytoplankton standing stocks in these so-called 'High-Nitrate Low-Chlorophyll' (HNLC) regions, John Martin suggested that growth limitation through insufficient availability of the micro-nutrient iron (Fe) might also exert an important control [*Martin and Fitzwater*, 1988]. He furthermore proposed that stimulation of biological productivity through increased aeolian Fe delivery to the Southern Ocean at the height of the last ice age might have led to the concurrently low levels observed of atmospheric CO_2 [*Martin*, 1990]. The

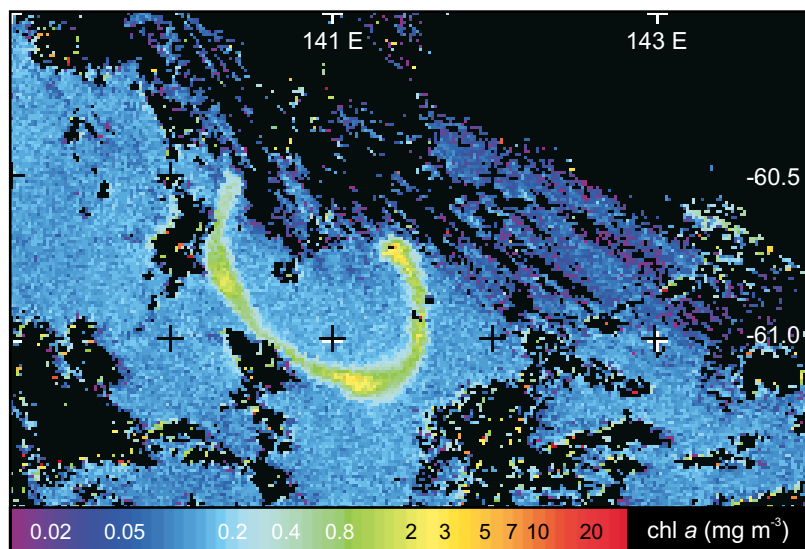


Figure 5-12 Image of the SOIREE bloom in the Southern Ocean in the region of 141°E 61°S, taken from the SeaWiFS ocean colour satellite on 23rd March 1999, some 6 weeks following initial Fe release [Abraham *et al.*, 2000]. The SeaWiFS data, provided by the NASA DAAC/GSFC and copyright of Orbital Imaging Corps and the NASA SeaWiFS project, was processed at CCMS-PML.

‘IronEx II’ open ocean Fe fertilization experiment demonstrated unequivocally the role that iron played in limiting phytoplankton growth (particularly of larger diatoms) in the equatorial Pacific [Coale *et al.*, 1996a,b]. More recently, a similar experiment (‘SOIREE’) was carried out in the Southern Ocean. Here too, an unambiguous response of the phytoplankton standing stock to the addition of Fe was observed [Boyd *et al.*, 2000].

To test the ‘Iron Hypothesis’ for low glacial $x\text{CO}_2$ it should be sufficient to increase aeolian deposition rates in the model and record the results. However, there is a caveat to the use of SUE in predicting the atmospheric response to Fe fertilization. This concerns the nature of the scheme for biological productivity in which export production is estimated directly from ambient nutrient concentrations with the aid of Michaelis-Menten kinetics (2.2.3). A response of POC export upon relief of Fe limitation is, therefore, implicitly assumed. Although increased export production was indeed reported in the equatorial Pacific as a result of Fe fertilization [Coale *et al.*, 1996b], there was no evidence during the 14-day course of SOIREE that POC export was similarly enhanced in the Southern Ocean [Boyd *et al.*, 2000; Charette and Buesseler, 2000] in spite of a significant draw-down in surface ocean $f\text{CO}_2$ having occurred [Boyd *et al.*, 2000; Watson *et al.*, 2000]. Furthermore, the apparent persistence of the bloom (on the basis of remotely-sensed elevated surface chlorophyll concentrations, as shown in Figure 5-12) for several months after the end of the experiment [Abraham *et al.*, 2000] implies that losses of Fe must have been relatively restricted over this entire period and thus export constrained to be modest. A very different response, though, might be expected from a continuous

enhancement of aeolian Fe supply over a period of thousands of years and across the entire Southern Ocean, as opposed to that obtained under the temporal and spatially-limited experimental conditions of SOIREE [Ridgwell, 2000]. Regardless of the specifics of Southern Ocean ecosystem dynamics, a more general response of the system to changes in aeolian Fe supply is to be expected. Accumulation rates of aeolian mineral material in deep-sea sediments around the world are generally higher during glacial periods than at present [Balsam *et al.*, 1995; deMenocal, 1995; deMenocal *et al.*, 1993; Pye, 1989; Rea *et al.*, 1986; Ruddiman, 1997]. This is supported by AGCM modelling studies, which predict that in the drier, colder, and windier glacial climate, dust transport from terrestrial sources to the open ocean is more efficient [Andersen *et al.*, 1998; Genthon, 1992; Mahowald *et al.*, 1999; Joussaume, 1993]. Furthermore, concurrent expansion of arid dust source areas [Adams *et al.*, 1990; Iriondo, 2000] would act so as to further enhance the flux of material to the ocean [Andersen and Ditlevsen, 1998; Mahowald *et al.*, 1999; Reader *et al.*, 1999]. Although the primary impact of increased aeolian Fe supply is on the enhancement of productivity (in HNLC regions) there are more subtle secondary effects that may be equally important in affecting $x\text{CO}_2$ over the longer term. Fe-replete conditions have been demonstrated to favour (predominantly larger) diatoms over pico- and nano-plankton [Boyd *et al.*, 2000; Coale *et al.*, 1996b; Watson *et al.*, 2000]. Since CaCO_3 is only produced by smaller phytoplankton (coccolithophorids), such a shift in species composition will reduce the CaCO_3 :POC rain ratio [Harrison, 2000; Watson and Lefèvre, 1999], driving enhanced

CaCO₃ dissolution in deep-sea sediments and thus lower $x\text{CO}_2$ [Archer and Maier-Reimer, 1994].

To test the hypothesis that glacial-interglacial changes in aeolian Fe supply to the ocean exerted a strong control over atmospheric composition, dust deposition fluxes to the ocean surface were altered. Present-day and LGM distributions of dust flux were taken from Mahowald *et al.* [1999]. The Vostok dust concentration record [Petit *et al.*, 1999] is used as a proxy for the timing and rate of change of deposition in order to reconstruct a record for the last 400 ka. Use of a signal template of dust deposition rates at Vostok (reconstructed using estimated snow accumulation rates [Petit, pers com]) as opposed to the dust concentration record makes very little difference.

The results of this exercise are summarized in Figure 5-13. The response of $x\text{CO}_2$ to this forcing is pronounced, with a 19→0 ka BP increase of 52.4 ppmv. There are several components that contribute to this: a fast response via the direct effects of changes in iron availability on export production (accounting for perhaps three quarters of the deglacial increase) together with a slower one, arising through adjustment of the deep-sea sediment system [Watson *et al.*, 2000]. The first component is associated with total POC export during the LGM being some ~10% higher than at present. There is also a shift in species composition with siliceous phytoplankton favoured (via increased Fe-driven efficiency in H₄SiO₄ utilization), suppressing CaCO₃ export by 24%. The second component involves a reduction in the CaCO₃ inventory of deep-sea surface sediments driven by a lower CaCO₃:POC rain ratio [Archer and Maier-Reimer, 1994]. This takes place more gradually with an adjustment time scale of ~9 ka. There is also a third component, although this is only apparent in the response of the system to an artificial stepped transition in dust supply. This involves a gradual depletion in oceanic H₄SiO₄ inventory under the influence of enhanced biogenic opal export. This acts so as to partly reverse the influence on atmospheric composition of the first two components, taking place with an *e*-folding time of ~25 ka (characteristic of direct perturbations made to the global Si cycle – see 5.4.8.3).

In addition to the model explaining slightly more than half the entire deglacial rise, there is an obvious marked similarity in shape between the time evolution of model and observed CO₂ concentrations. In particular, the model can explain virtually all the variability associated with full glacial periods (e.g., Stages 4 through 2). $\delta^{13}\text{C}^{\text{CO}_2}$ also exhibits a response consistent with early observed deglacial change, with a fall of some 0.19‰ over the interval 19→0 ka BP. However, an extremely marked response is exhibited by the calcite lysoclines (Figure 5-13d,e). Associated with episodes of high dust deposition is intense dissolution and dilution (by increased detrital input) of calcite virtually throughout the depth of the water column, both in the Atlantic and Pacific basins. A perturbation of sedimentary composition of this magnitude is greater than can be supported by available paleoceanographic evidence, at least for the Pacific. There are a number of possible explanations for this mismatch:

- Glacial dust supply might be over-estimated.

- The simplistic zonally-averaged ocean circulation might lead to variability in mid-latitude export production being over-sensitive to changes in global Fe availability.
- The biological export scheme might be producing an unrealistic response of the CaCO₃:POC rain ratio to changes in Fe availability.
- The component of sedimentary CaCO₃ dissolution driven by the respiration of POC might be over-estimated.
- General deficiencies in the global CaCO₃ cycle, with insufficient burial of CaCO₃ in the benthic environment.

In light of these uncertainties the effect on atmospheric composition of whole-ocean changes in dust deposition should be considered as an upper limit of possible response.

5.4.10 The nitrogen hypothesis

Although it can't be directly assessed in SUE, the oceanic nitrogen cycle has been suggested to be a potentially significant element in the dynamical evolution of the global carbon cycle over the late Quaternary. Various hypotheses have been forwarded to explain the observed glacial-interglacial variability in atmospheric composition, all envisioning in some way or other an oceanic NO₃ inventory higher during glacial periods than interglacials. Comparisons made between the predictions of ocean N cycle models and paleoceanographic $\delta^{15}\text{N}$ proxy data go some way to supporting this assertion [Altabet and Curry, 1989].

Hypotheses forwarded for the rapid rise in $x\text{CO}_2$ at deglacial inception require the existence of a critical threshold within the oceanic nitrogen cycle. In this, during the descent into full glacial climate, dissolved O₂ concentrations in the ocean gradually fall until at some point widespread denitrification rapidly proceeds. Since the oceanic residence time of NO₃ is relatively short (3-10 ka [Codispoti, 1995]) the oceanic nitrate inventory could be quickly depleted, resulting in decreased biological productivity and thus a steep rise in atmospheric CO₂ [Knox and McElroy, 1984; Shaffer, 1990]. Declining [O₂] could be driven by increased productivity fuelled by nutrients (PO₄ and/or NO₃) eroded from shelf sediments exposed as sea level falls [McElroy, 1983; Shaffer, 1990].

A second hypothesis draws its basis from the likelihood that the modern ocean nitrogen cycle is far from steady state, with nitrogen losses from the ocean through denitrification (particularly on continental shelves) exceeding the combined input from rivers, atmosphere, and nitrogen fixation in the surface ocean [Berger and Vincent, 1986; Codispoti, 1995; McElroy, 1983]. With sea level fall, denitrification within neritic sediments ceases on the newly exposed shelf area. This leads to an increase in the oceanic N inventory, which fuels greater productivity leading to CO₂ draw-down [Altabet and Curry, 1989; Berger and Vincent, 1986; Codispoti, 1995; Ganeshram *et al.*, 1995]. Although this mechanism can correctly generate CO₂ draw-down as glaciations intensify, deglacial CO₂ rise will lag sea level change contrary to observed temporal relationships, barring it from being a stand-alone explanation.

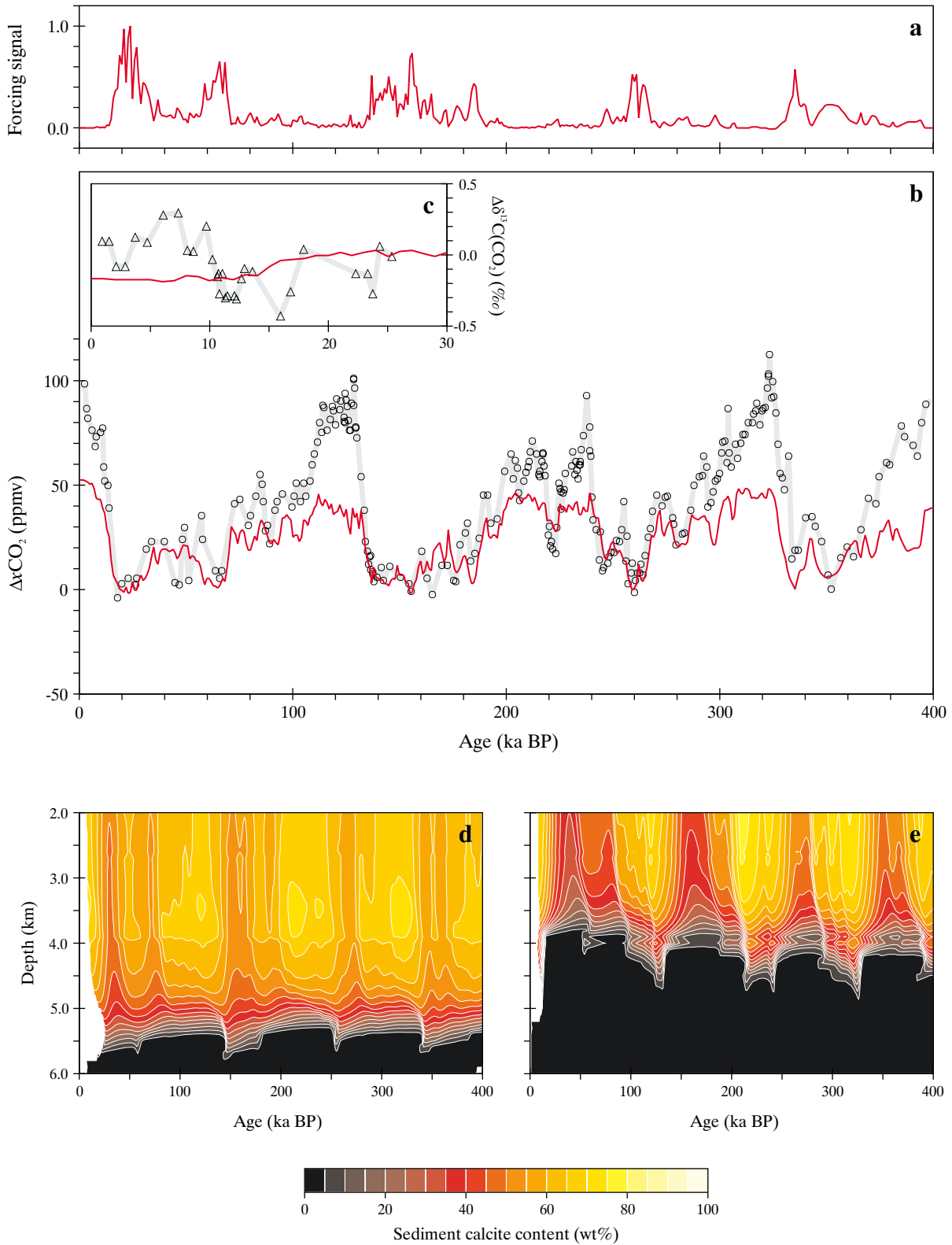


Figure 5-13 Effects on the global carbon cycle of glacial-interglacial variability in dust deposition to the world ocean. Shown are; (a) the forcing signal (normalized to a value of unity at the LGM); (b) model $\Delta x\text{CO}_2$ response (red line) compared to the Vostok ice core record [Petit *et al.*, 1999] (grey line with data points); (c) model $\delta^{13}\text{C}^{\text{CO}_2}$ response (red line) compared to the Taylor Dome ice core record [Smith *et al.*, 1999] (grey line with data points); (d) and (e) the response of the calcite lysocline in the (south) Atlantic and (south) Pacific basins, respectively.

Recently, a third variant has been suggested whereby increased Fe availability arising from aeolian dust deposition simulates the activity of diazotrophs such as *Trichodesmium* spp. in the surface ocean, thereby increasing the rate of N₂ fixation [Broecker and Henderson, 1998; Falkowski, 1997]. As a consequence, biological productivity and thus CO₂ draw-down follow (lagged) changes in aeolian dust supply, in general agreement with ice core records.

All these require as a minimum a detailed representation of the oceanic nitrogen cycle. However, this is still relatively poorly understood, particularly in terms of the rates and locations of nitrogen fixation and denitrification in the ocean. These in turn are critically dependent on seasonal and transient [O₂] and [Fe] distributions in the ocean, both of which are beyond the capability of the model configurations developed in the present study to reproduce sufficiently well for this purpose.

5.5 The role of the Southern Ocean

The Southern Ocean has long been regarded as a pivotal region for glacial-interglacial change in the global carbon cycle, with mechanisms relating to increased biological productivity [Knox and McElroy, 1984; Martin, 1990; Sarmiento and Toggweiler, 1984], decreased vertical mixing rates [Francois et al., 1997; Sigman et al., 1999a,b], increased wind speed [Keir, 1993a,b], and greater sea ice cover [Broecker and Peng, 1986; Moore et al., 2000; Stephens and Keeling, 2000] all having been proposed as playing important roles. The Southern Ocean achieves its climatic status both biochemically, as a result of the pool of excess nutrients found there [de Baar and Boyd, 2000], and through its physical oceanographic characteristics as a pathway of relatively low resistance linking the carbon reservoirs of the atmosphere and deep ocean [Sarmiento and Toggweiler, 1984]. Mechanisms influencing the carbon cycle relating to changes in biological productivity and sea ice extent in this region are now investigated in more detail with the aid of the higher resolution model implementation, SUE2108 (4.5), and constrained through consideration of additional paleoceanographic proxies.

5.5.1 Glacial-interglacial variability in dust deposition

John Martin's glacial Fe fertilization hypothesis [Martin, 1990], formulated specifically with regards to the Southern Ocean is now tested. For this, dust deposition is only varied within the Southern Ocean, defined as ocean area south of 47.5°S (Figure 4-1). Restricting Fe fertilization in this way avoids many of the possible biases suspected to arise from whole-ocean dust forcing (5.4.9). Variability in atmospheric composition thereby obtained will now represent a minimum likely effect of whole-ocean change in dust deposition, particularly since the HBEI score of the model suggests that the role of the Southern Ocean in controlling $x\text{CO}_2$ may be underestimated (5.3.1). As before, the magnitudes of

deposition flux under modern and LGM conditions is taken from Mahowald et al. [1999] with the forcing signal following Vostok dust concentrations [Petit et al., 1999].

The results of this exercise are summarized in Figure 5-14. The response of $x\text{CO}_2$ to declining dust fluxes in the Southern Ocean is an increase of 21.9 ppmv over the interval 19→0 ka BP with an associated decrease in $\delta^{13}\text{C}^{\text{CO}_2}$ of 0.15‰. Glacial draw-down in $x\text{CO}_2$ is a consequence of POC export being enhanced by ~100% south of about 54°S driven by increased Fe-availability. Although export from siliceous phytoplankton dominates this response (>95%), opal export increases by no more than ~35% due to greater Si utilization efficiency (enabled by higher ambient dissolved Fe levels). As a result of greater macro-nutrient utilization in the Southern Ocean there is decreased advective nutrient supply to the north, reducing POC export at lower latitudes. This slightly offsets $x\text{CO}_2$ draw-down driven by the Southern Ocean alone. In contrast to the significant response obtained in this study, box models of ocean Fe cycling have predicted that an increase in dust supply of order 1000 is required to produce a comparable decrease in $x\text{CO}_2$ [Lefèvre and Watson, 1999]. However, boundary conditions for this were taken from the Duce et al. [1991] dust deposition field such that the supply of Fe to the modern surface Southern Ocean was almost entirely from below (~99%). Although adoption of a similar depositional field might diminish the response in SUE1608, aeolian Fe solubilities assumed here are relatively low and could be substantially increased (countering lower dust fluxes) without degrading the plausibility of model assumptions. This present study also differs from results obtained from a coupled ecological and ocean box model which suggested that a realistic lifting of Fe limitation in the Southern Ocean would produce a draw-down in $x\text{CO}_2$ of only 12 ppmv [Popova et al., 2000]. However, this draw-down resulted from an increase in global new production of 1.7 GtC a⁻¹. That an increase in new production only slightly higher (2.2 GtC a⁻¹) obtained upon the lifting of physical constraints on productivity in the Southern Ocean in a 3D OGCM produced a draw-down of 34 ppmv [Kurz and Maier-Reimer, 1993] suggests that the relatively simple ocean model of Popova et al. [2000] may be overly insensitive to high latitude perturbations.

The general shape of the response of atmospheric composition over the course of the late Quaternary is noticeably different from that arising from whole ocean changes in dust flux (Figure 5-13). In particular, peak Holocene $x\text{CO}_2$ appears to be centred on ~7 ka BP. Since Fe-fertilization now takes place away from ocean regions overlying CaCO₃-rich sediments, there can be relatively little direct control exerted on CaCO₃ dissolution, with only modest changes in lysocline depth occurring (Figure 14d,e). The effect of the gradual recovery in oceanic H₄SiO₄ inventory following its previous glacial draw-down is now revealed – increasing H₄SiO₄ availability over the course of the Holocene shifts species composition towards siliceous phytoplankton which in turn produces a negative pressure on $x\text{CO}_2$, dominating the atmospheric response once the decline in dust flux has virtually ceased. The poor reproduction of the general trend observed in $x\text{CO}_2$ from Stage 5e through 2

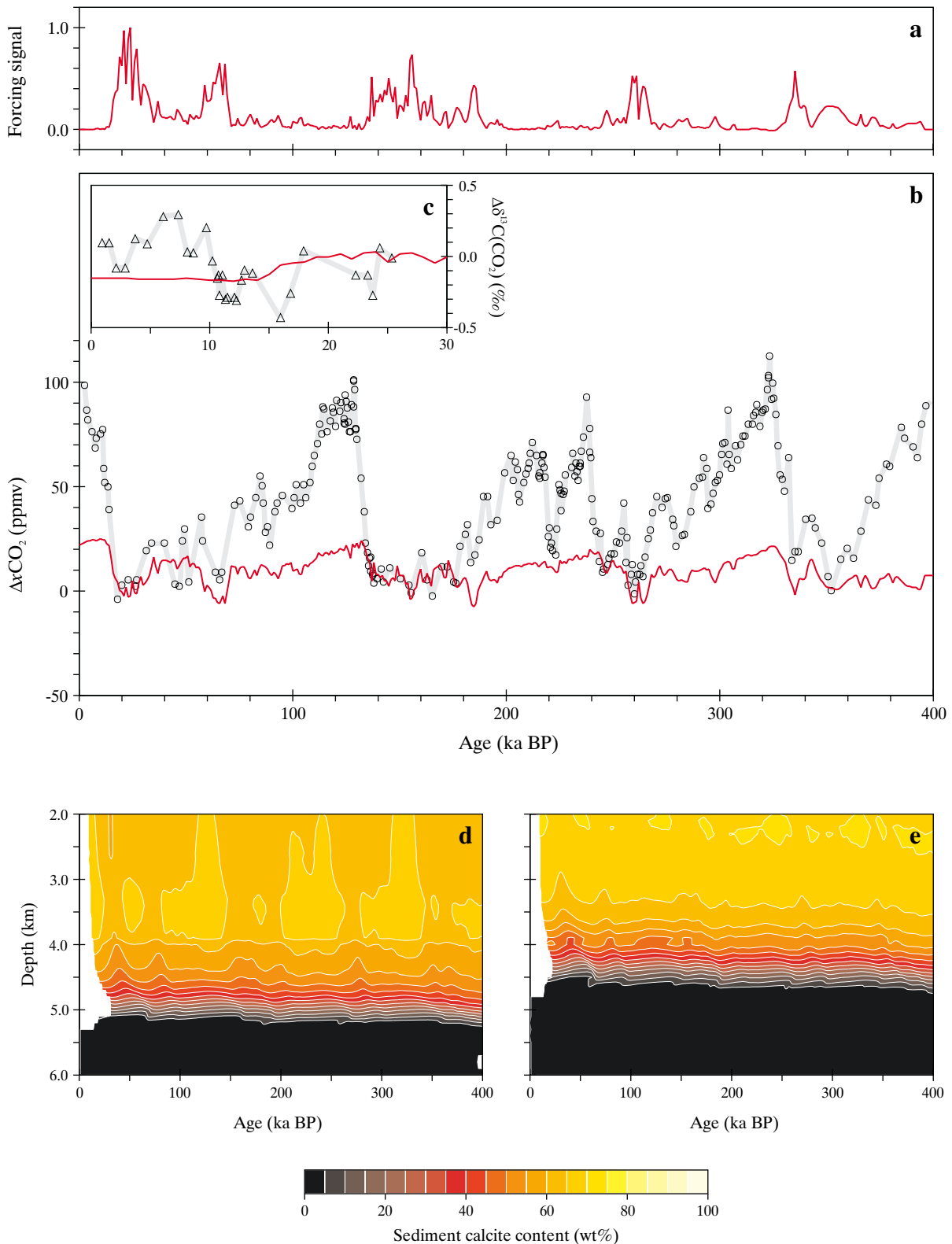


Figure 5-14 Effects on the global carbon cycle of glacial-interglacial variability in dust supply to the Southern Ocean. Shown are; (a) the forcing signal (normalized to a value of unity at the LGM); (b) model $\Delta x\text{CO}_2$ response (red line) compared to the Vostok ice core record [Petit *et al.*, 1999] (grey line with data points); (c) model $\delta^{13}\text{C}(\text{CO}_2)$ response (red line) compared to the Taylor Dome ice core record [Smith *et al.*, 1999] (grey line with data points); (d) and (e) the response of the calcite lysocline in the (south) Atlantic and (south) Pacific basins, respectively.

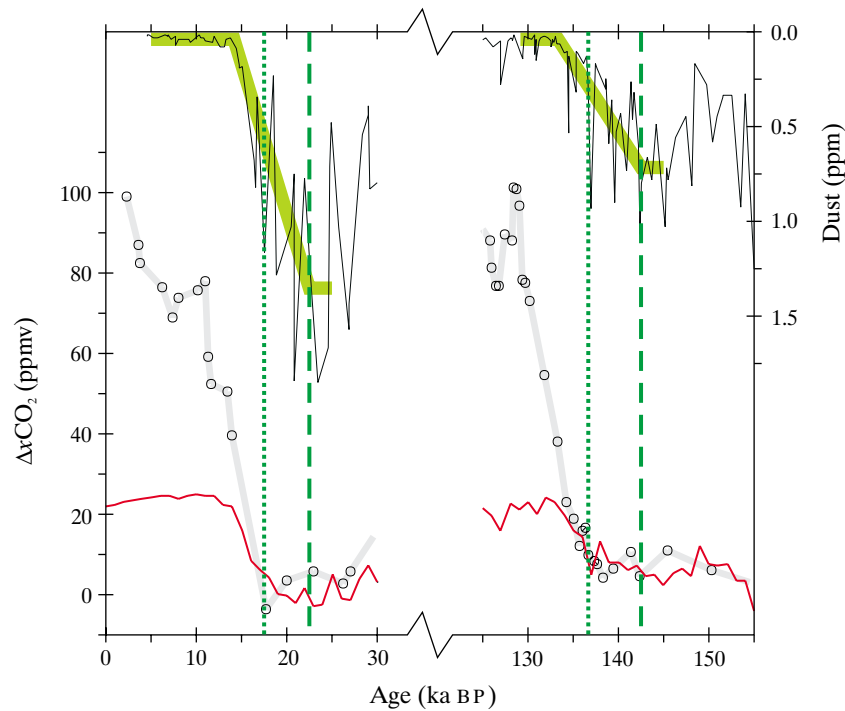


Figure 5-15 Temporal relationships surrounding glacial Terminations I and II between observed dust (thin black line, inverted at top) and CO₂ concentrations contained within the Vostok ice core (thick grey line with data points) [Petit *et al.*, 1999] and model xCO₂ (red line). The general decreasing trend in dust concentrations associated with the deglacial transition is highlighted in green, with the start of this dust decline marked by a dashed line, and the start of CO₂ rise by a dotted line.

is partly due to the same effect, whereby a gradually decreasing H₄SiO₄ inventory works against CO₂ draw-down driven by increasing Fe availability in the Southern Ocean. The maximum glacial-interglacial contrast associated with Termination I is therefore some 27.7 ppmv (over 23→7 ka BP) with 0.19‰ in δ¹³C^{CO₂}.

Probably the most compelling aspect of the model atmospheric CO₂ response to dust variability concerns the timing of the major perturbations [Watson *et al.*, 2000]. Figure 5-15 shows the events surrounding the last two glacial terminations on an expanded time scale. It can be seen that there is an excellent temporal match (within ~1 ka) between the onset of periods of rapid xCO₂ rise in both modelled and observed signals. This is despite dust deposition fluxes having begun to decline at least 5 ka before this point, with little associated increase in xCO₂. This lag has previously been interpreted by Broecker and Henderson [1998] as a powerful argument against John Martin's hypothesis. That a system as complex as the global carbon cycle should be highly non-linear in this respect should hardly be surprising. Non-linearities arise in the model through a number of factors:

- Onset of (summer-time) H₄SiO₄ limitation in the more northerly reaches of the Southern Ocean.
- Through Michaelis Menten saturation kinetics in the biological export model, whereby further increases in export start to tail off rapidly with increasing Fe

availability once half saturation concentrations have been surpassed.

- Increasing loss of Fe from the surface ocean through both 'self-scavenging' (2.2.5) and decreasing efficiency of Fe use by phytoplankton (i.e., increasing organic matter Fe:C ratios - see Figure 2-2).

These combine to produce the observed behaviour with POC export declining rapidly (and thus increasing xCO₂) once dust deposition fluxes start to drop below a critical level. A degree of variability can still be observed even during peak glacial times. However, because the amplitude of the response during this time is highly dampened, an apparent lag is produced between the start of dust decline and significant CO₂ rise as observed by Broecker and Henderson [1988].

Paleoceanographic evidence from the Southern Ocean reveals a fundamental meridional divide, with glacial-interglacial changes in the opal content of deep-sea sediments either side of the position of the present-day Antarctic Polar Front (APF) being virtually opposite in sign. To the south, glacial-age sediments are characterized by a lower opal content than during interglacial periods, while to the north, it is interglacial sediments that are the more opal-rich [Anderson *et al.*, 1998; Charles *et al.*, 1991; De La Rocha *et al.*, 1998; Francois *et al.*, 1997; Kumar *et al.*, 1995; Mortlock *et al.*, 1991]. Although changes in preservation efficiency, sediment focussing, and the physiological effects

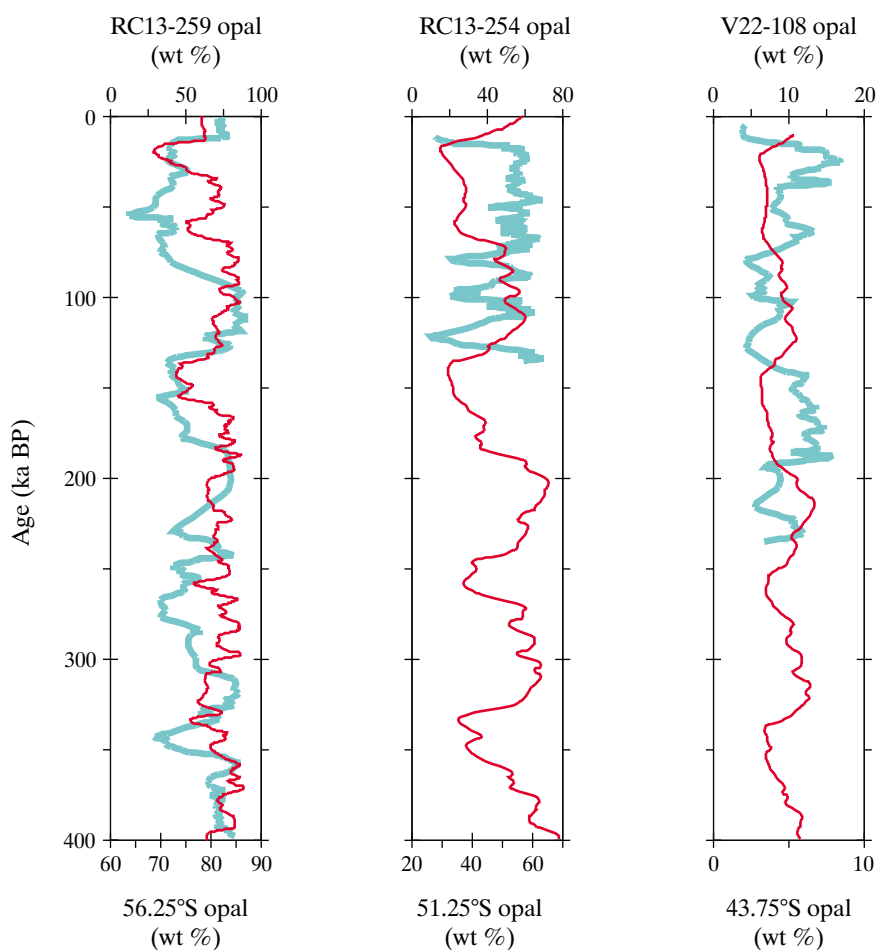


Figure 5-16 Observed variability in sedimentary opal content from a transect spanning the approximate location of the modern Antarctic Polar Front in the Atlantic sector of the Southern Ocean [Mortlock *et al.*, 1991] (blue) compared to synthetic model sediment core results (red) generated by SUE2108 and forced by glacial-interglacial variability in dust deposition to the Southern Ocean.

of Fe availability on diatoms can all complicate the interpretation of this [Anderson *et al.*, 1998; Boyle, 1998; Francois *et al.*, 1997; Takeda, 1998], indicators of H_4SiO_4 utilization in the surface ocean such as opal Ge/Si ratios [Froelich *et al.*, 1989; Mortlock *et al.*, 1991] and $\delta^{30}\text{Si}$ [De La Rocha *et al.*, 1998] are consistent at least with the sign of the observed change in opal content. This coupled antagonistic response presents us with an important validation target for proposed carbon cycle mechanisms operating in the Southern Ocean.

Figure 5-16 shows down-core variability in opal content in three cores spanning the APF in the Atlantic sector of the Southern Ocean [Mortlock *et al.*, 1991]. Core RC13-259 (53°53'S) is located to the south of the APF while RC13-254 (48°34'S) and V22-108 (43°11'S) both come from further to the north. Also shown are records of down-core opal content contained within synthetic sediments cores located at the nearest equivalent model grid points. It can be seen that while deglacial increases in %opal are reproduced by the model for Terminations I and II in RC13-259 there is little

other correspondence with this core. For the two cores located to the north of the APF the situation is far worse, with the model exhibiting a distinct anti-phase relationship with paleoceanographic observations. Low glacial opal content in these two synthetic cores is a direct consequence of local nutrient limitation, as macro-nutrients previously advected northwards across the APF are depleted under the influence of Fe-fertilization to the south. Clearly, either the effect of Fe fertilization in the Southern Ocean is being substantially overstated in the model, or one or more mechanisms important to the paleoceanographic record in the Southern Ocean have not been accounted for.

5.5.2 The role of changes in seasonal sea ice extent

It was shown earlier that, in isolation, changes in the maximum seasonal limits of sea ice extent in the Southern Ocean have little direct impact on the concentration of atmospheric CO_2 . However, such changes might be critical in

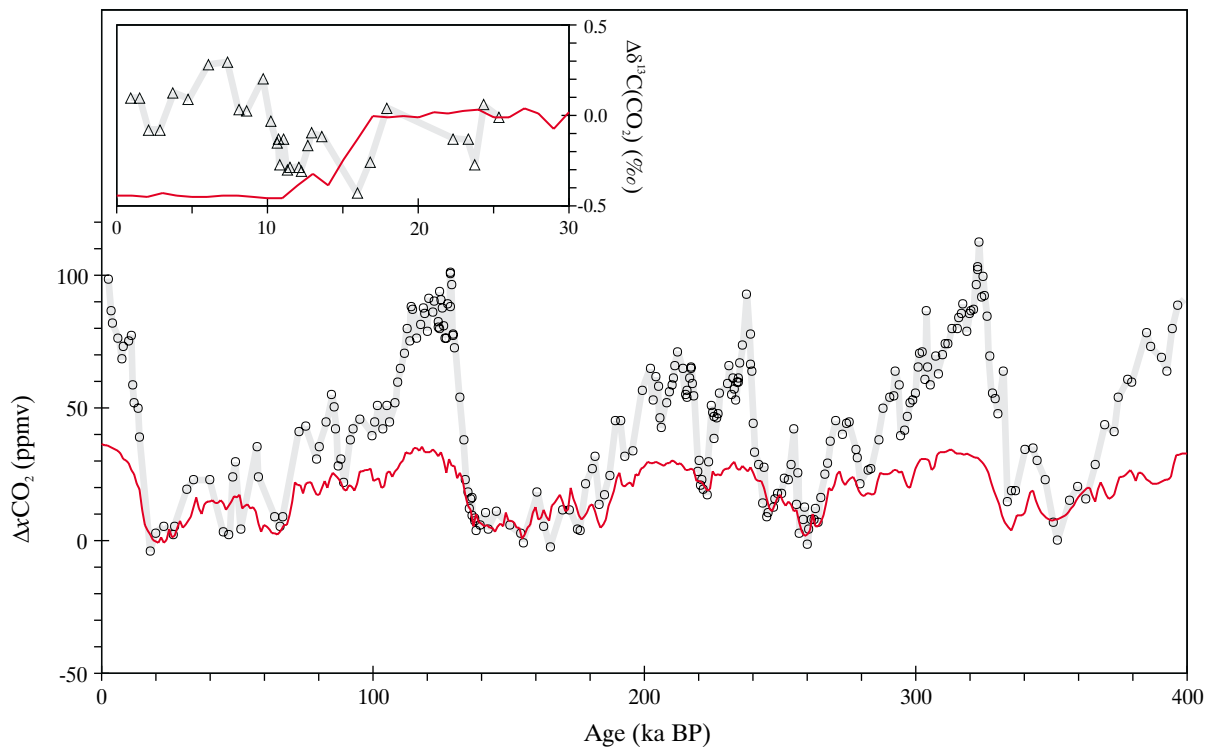


Figure 5-17 Effects on the global carbon cycle of glacial-interglacial variability in both dust deposition to the Southern Ocean and sea ice extent. Shown is the model $x\text{CO}_2$ response (red line) compared to the Vostok ice core record [Petit et al., 1999] (grey line with data points) with inset – model $\delta^{13}\text{C}^{\text{CO}_2}$ response (red line) compared to the Taylor Dome ice core record [Smith et al., 1999] (grey line with data points).

explaining some of the observed paleoceanographic features of this region [Charles et al., 1991]. Fractional sea ice cover is, therefore, now varied in addition to changes in dust deposition. A record of sea ice cover is reconstructed for the past 400 ka as before (5.4.4), taking maximum (winter-time) and minimum (summer-time) coverage for each grid point region from the CLIMAP [1984] and taking Vostok δD [Petit et al., 1999] as a signal template.

The response of atmospheric composition to this combined forcing is shown in Figure 5-17. During glacial periods, the presence of increased seasonal sea ice cover south of the APF results in much lower POC export, with a complete cessation south of about 62.5°S . Importantly, sea ice cover prevents escape of CO_2 to the atmosphere during non-productive winter months. Previously utilized macro-nutrients are advected northwards, fuelling much greater ($>100\%$) POC export just to the north of the APF in conjunction with higher Fe availability. The combination of these factors helps to enhance the glacial-interglacial contrast in $x\text{CO}_2$ to 36.3 ppmv (19→0 ka BP). The overall form of the model $x\text{CO}_2$ signal now bears a noticeably closer resemblance to the Vostok record than through Fe fertilization alone, particularly in the relative levels along the sequence of transitions Stage 5e through Stage 2. The full $\sim 0.4\%$ decrease observed in $\delta^{13}\text{C}^{\text{CO}_2}$ associated with deglacial inception can also now be accounted for.

The addition of varying sea ice extent brings about a remarkable change in the synthetic opal sediment records (Figure 5-18), with most of the major transitions in opal content reproduced extremely well (even the characteristic antagonistic variability either side of the APF). Although there is a substantial mismatch between model and observations during Stages 3 and 4 in RC13-259, this core has a known hiatus around this level [Anderson, pers comm], which could easily account for this. The correspondence in the timing of the changes are all the more surprising considering that the synthetic model age scale and that derived on the basis of $\delta^{18}\text{O}$ stratigraphy in the observed records are unlikely to be equivalent. Indeed, by eye, RC13-254 appears to share an even greater similarity in opal variability with the paired synthetic model record than it does with core V29-105, located only $0^\circ 29'$ further to the north [Mortlock et al., 1991]. Absolute values of opal content do not correspond nearly so well, particularly for core RC13-254. However, this is not entirely unexpected since model sediments represent zonal means whilst individual deep-sea sediment cores record local conditions.

With regard to other paleoceanographic proxy evidence from the Southern Ocean, the model predicts generally lower glacial POM export well to the south of the APF compared to at present but becomes largely invariant with respect to the deglacial transition as the APF is approached.

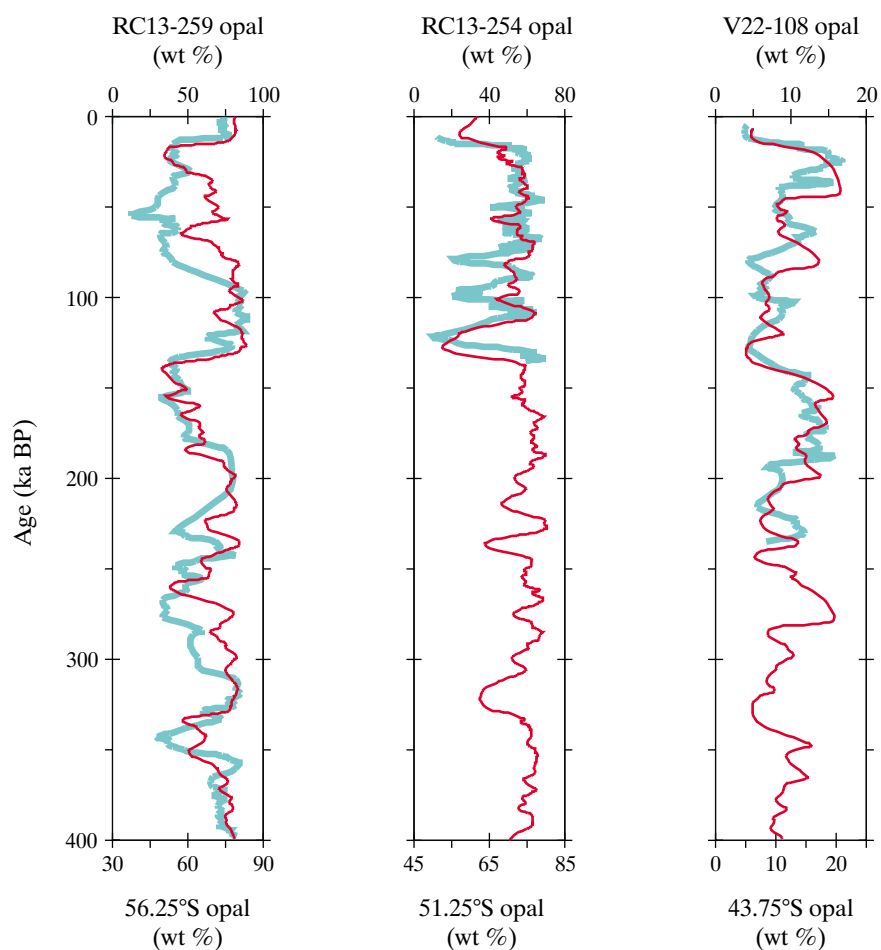


Figure 5-18 Observed variability in sedimentary opal content from a transect spanning the approximate location of the modern Antarctic Polar Front in the Atlantic sector of the Southern Ocean [Mortlock *et al.*, 1991] (blue) compared to synthetic model sediment core results (red) generated by SUE2108 and forced by glacial-interglacial variability in both dust deposition to the Southern Ocean and sea ice extent.

This is consistent with organic matter export proxies such as $^{231}\text{Pa}/^{230}\text{Th}$ and $^{10}\text{Be}/^{230}\text{Th}$ ratios, authigenic U production, and Ba accumulation fluxes [Anderson *et al.*, 1998; Francois *et al.*, 1997; Kumar *et al.*, 1995]. As a result, annual mean PO_4 concentrations are at their highest levels during the LGM, in line with lower PO_4 utilization suggested by Cd/Ca ratios [Elderfield and Rickaby, 2000; Rickaby and Elderfield, 1999]. In addition, the synthetic sediment record exhibits a deglacial (19→0 ka BP) rise in planktonic foraminiferal $\delta^{13}\text{C}$ of $\sim 1.0\text{‰}$ at 56.25°S (not shown), virtually identical to the change recorded in RC13-259 [Mortlock *et al.*, 1991].

To the north of the APF the model also performs well against additional observational indicators. Substantially higher glacial POM export is again consistent with $^{231}\text{Pa}/^{230}\text{Th}$, $^{10}\text{Be}/^{230}\text{Th}$, authigenic U production, and Ba accumulation records, as well as with phytoplankton biomarkers [Anderson *et al.*, 1998; Francois *et al.*, 1997; Ikehara *et al.*, 2000; Kumar *et al.*, 1995]. Although temperature-corrected changes in sub-Antarctic Cd/Ca ratios have been interpreted as indicating a fairly minimal change

in surface ocean PO_4 concentrations [Elderfield and Rickaby, 2000], uncertainties in this proxy allow for a reduction during the LGM of up to $0.5 \mu\text{mol kg}^{-1}$, agreeing with a mean annual glacial draw-down in the model at 51.25°S and 43.75°S of ~ 0.4 and $\sim 0.3 \mu\text{mol kg}^{-1}$, respectively.

However, there is one further paleoceanographic indicator conspicuous by its absence in the discussion so far. Changes in the ^{15}N isotopic composition of organic matter, a proxy for surface ocean nitrate utilization, is difficult to reconcile with the interpretation of other nutrient and export proxies in this region. Indeed, $\delta^{15}\text{N}$ suggests almost the complete opposite, with increased glacial nutrient utilization south of the APF and decreased or unchanged utilization to the north [Francois *et al.*, 1997; Sigman *et al.*, 1999a,b]. Factors controlling productivity proxies are therefore probably much less well understood than was previously assumed [Cullen *et al.*, 1999; Sigman and Boyle, 2000]. In the case of $\delta^{15}\text{N}$ it is possible that the observed variability may be significantly affected by factors other than the degree of nitrate utilization. For instance, increased export production due to

prymnesiophytes such as *Phaeocystis antarctica* might radically alter N/P uptake ratios and thus decouple nitrate utilization from POC export, while the different ^{15}N fractionation regime associated with sea ice algal communities might distort the mean $\delta^{15}\text{N}$ signal [Elderfield and Rickaby, 2000].

5.6 Towards the complete picture

It is apparent, at least for the hypotheses tested in this present study that no single mechanisms can simultaneously fulfill the constraints dictated even by the limited paleoclimatic evidence considered so far. The explanation for the observed glacial-interglacial variability in the concentration of atmospheric CO_2 must therefore lie in a combination of processes at work together over the course of the late Quaternary. Indeed, it has already been shown that through combining changes in sea ice extent with dust deposition in the Southern Ocean it is possible to correctly account for a number of key paleoatmospheric and paleoceanographic features. Although in this case the influence on $x\text{CO}_2$ of sea ice in isolation is limited, its addition to dust deposition forcing is evidently non-linear, producing a marked improvement in the amplitude and overall character of the resulting $x\text{CO}_2$ signal. Mechanisms that in isolation appear to have little impact may therefore actually play an essential role as a component of wider change in the global carbon cycle. It is therefore important that even effects that are superficially ‘unhelpful’ in reproducing the observed atmospheric signal, such as CO_2 draw-down forced by deglacial increases in terrestrial carbon storage, must be included in order to build up a complete picture of the evolution of the system. All the separate mechanisms tested so far are now combined.

SUE2108 is run with the ocean carbon cycle forced by the following perturbations:

- sea level change (117 m 19→0 ka BP rise with a 1.05‰ decrease in ocean salinity) and following SPECMAP
- ocean surface temperature changes (19→0 ka BP difference taken from CLIMAP, but with LGM tropical temperatures cooler by an additional 2°C), with the NH weighted according to SPECMAP and the SH to Vostok δD .
- wind speed changes in the SH only, weighted to Vostok Na concentrations
- variability in sea ice extent (19→0 ka BP difference taken from CLIMAP) in the SH only, weighted to Vostok δD
- changes in Atlantic overturning circulation (19→0 ka BP difference taken from the two alternative circulations of the Bern 2D ZOGCM [Marchal, pers comm]) and following SPECMAP
- changes in terrestrial carbon storage (500 GtC 19→0 ka BP increase) following SPECMAP
- changes in neritic CaCO_3 storage (50% strength of the parameterization of Munhoven and Francois [1996])
- 6.6% solubility of SiO_2 (present at 66 wt%) in aeolian dust deposited to the ocean surface, and a variable sink

in neritic opal accumulation rate (19→0 ka BP increase of $\sim 0.8 \text{ Tmol Si a}^{-1}$)

- variability in aeolian Fe deposition to the Southern Ocean (19→0 ka BP decrease from Mahowald *et al.* [1999]) and following Vostok dust concentration changes.

In order to account for the fact that by simply ‘poisoning’ NADW formation (in order to produce the alternative circulation in the Bern 2D model) north Atlantic circulation does not shift southwards, sea ice extent is not extended in this composite scenario. To prevent overall glacial gas transfer rates in this region from then being overestimated wind speeds are also held invariant. The ocean carbon cycle is configured with a reduced POC-driven dissolution component to deep-sea sediment CaCO_3 diagenesis (5.4.7.1).

The results of this exercise are summarized in Figure 5-19. It can be seen that when combined these mechanisms can explain around two thirds of the observed variability in $x\text{CO}_2$, with a deglacial (19→0 ka BP) increase of some 61.1 ppmv. However, there are a number of specific areas where the model noticeably falls short with respect to the Vostok record. In particular, the initial rapid deglacial increase in $x\text{CO}_2$ surrounding Terminations I through III is significantly underestimated, there is too little intra-glacial variability (e.g., Stages 4 through 2), and the magnitude of the overall decline from interglacial to full glacial is lacking. A deglacial minimum in $\delta^{13}\text{C}^{\text{CO}_2}$ around ~ 15 ka BP is successfully predicted by the model, although it is less than half of the observed magnitude.

What are the reasons for the model-observation mismatches? Dealing with deglacial inception first, a critical aspect of combining together different model forcings which has not yet been fully considered is the relative phase between them [Henderson and Slowey, 2000]. The temporal evolution of boundary conditions of the northern hemisphere have, up until now, been assumed to mirror changes in the SPECMAP $\delta^{18}\text{O}$ stack [Imbrie *et al.*, 1984]. However, this record is a composite of mainly planktonic foraminifera and is not corrected for changes in ocean temperature. Rates of change predicted by this record and the timing of the mid-point of the deglacial transition, while sufficient for the investigation of the magnitude of glacial-interglacial change and to define long-term trends arising from single mechanisms, is unlikely to be adequate in a composite environment. Of particular concern in this regard is when (and how rapidly) increases in carbon stored in terrestrial ecosystems occur, since this acts so as to oppose the general trend of deglacial CO_2 increase. Indeed, it is noticeable that the model is more successful in predicting observed $x\text{CO}_2$ variability further back than ~ 250 ka BP, a period when the SPECMAP and Vostok time scales appear to be significantly out of sync.

An improved temporal framework for forcing the composite scenario over the course of Termination I can be devised by deriving signal templates for NH-weighted change from proxy signals taken from the GRIP Greenland ice core in leu of SPECMAP. Following Blunier *et al.* [1997], the GRIP ice core is placed onto the same age scale as the Vostok CO_2 target by matching changes in CH_4 concentrations surrounding the Younger Dryas event as

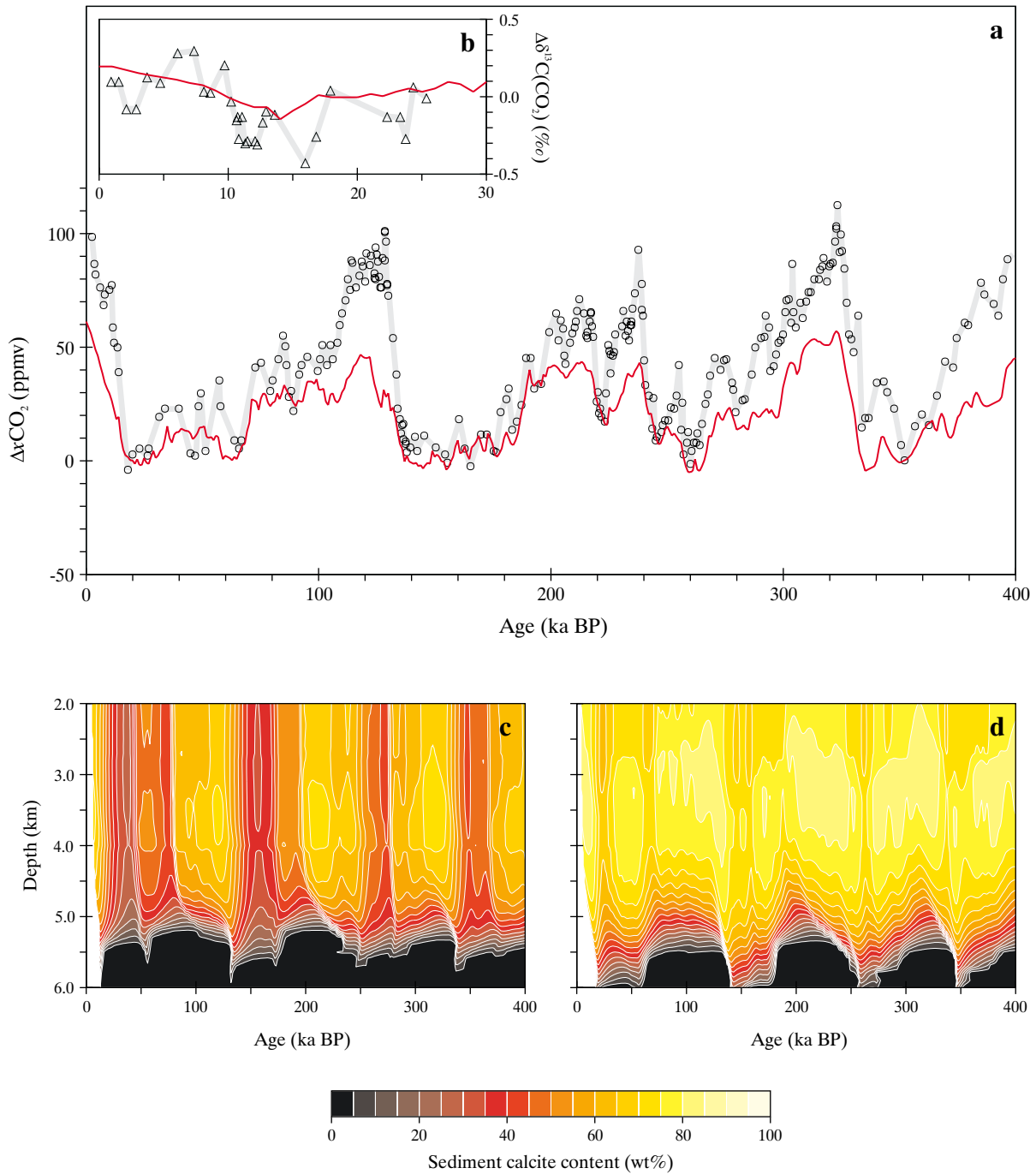


Figure 5-19 Effects on the global carbon cycle of a composite scenario for glacial-interglacial change. Shown are; (a) model $x\text{CO}_2$ response (red line) compared to the Vostok ice core record [Petit *et al.*, 1999] (grey line with data points); (b) model $\delta^{13}\text{C}(\text{CO}_2)$ response (red line) compared to the Taylor Dome ice core record [Smith *et al.*, 1999] (grey line with data points); (c) and (d) the response of the calcite lysocline in the (south) Atlantic and (south) Pacific basins, respectively.

recorded in these two cores. The $\delta^{18}\text{O}^{\text{ice}}$ record [Johnsen *et al.*, 1997], a proxy for local (air) temperature, is adopted to describe the evolution of NH-weighted SSTs over the last 20 ka together with changes in the Atlantic overturning circulation. The deglacial evolution of sea level is taken from Fairbanks [1989] and placed onto a common chronology with the other forcing records by linearly transforming ^{14}C ages so that the period separating meltwater pulses 1A and 1B corresponds with the Younger Dryas, as defined by GRIP $\delta^{18}\text{O}^{\text{ice}}$. Estimating the past history of changes in the size of the terrestrial biosphere carbon reservoir is much more difficult. While variations in atmospheric CH_4 concentrations relate to changes in terrestrial ecosystems, much of the magnitude of $x\text{CH}_4$ variability over the deglacial transition is thought to relate to changes in low latitude wetland extent [Blunier *et al.*, 1995] and thus predominantly reflect rapid changes occurring in local (tropical) hydrological regime rather than global biomass. Sea level rise (Fairbanks [1989]) is instead taken as a proxy for global biospheric state, but lagged with an e -folding time of 2 ka to account for the time taken for climax ecosystems to develop and soil carbon levels to stabilize. The maximum deglacial (19→0 ka BP) change is scaled to 500 GtC as before (5.4.6).

The effect on atmospheric composition of the new Termination I forcing chronologies is shown in Figure 5-20. It can be seen that the model now explains slightly more of the initial rapid increase in $x\text{CO}_2$ with the hiatus in CO_2 rise surrounding the Younger Dryas reproduced. However, even with this improved inter-hemispheric chronology the model still only accounts for almost 50% of CO_2 rise surrounding deglacial inception. With respect to $\delta^{13}\text{C}^{\text{CO}_2}$ the improvement is also partial. Again, the hiatus of the Younger Dryas period is reproduced but the initial transient is shallower than observed. It is likely that the relative chronologies of the forcings may still not reflect the real sequence of events. In particular, it is possible that collapse in sea ice extent was either slightly earlier or much more rapid than changes recorded by local temperature (as indicated by Vostok δD). This would enable a much more pronounced early minimum in $\delta^{13}\text{C}^{\text{CO}_2}$. Changes in convective regime, particularly if resulting in a greater degree of exposure of the atmosphere to the deep ocean would also enhance the respective responses in both $x\text{CO}_2$ and $\delta^{13}\text{C}^{\text{CO}_2}$. In addition, buildup in carbon stored in the terrestrial biosphere might be more sluggish still.

A second aspect of apparent deficiencies in predicted $x\text{CO}_2$ concerns the inherent sensitivity of model response. It has already been seen that according to indices of inter-regional control of levels of $x\text{CO}_2$ (5.3), SUE2108 has a tendency to under-estimate the importance of that high latitude regions of the world ocean. At least part of the missing response at deglacial inception and in intra-glacial variability (especially Stages 4 through 2) might then be due to an underestimation of mechanisms such as Fe fertilization in the Southern Ocean. Likewise, the model may be too insensitive to changes in fractional sea ice cover, particularly should the Southern Ocean actually be a stronger source of CO_2 to the atmosphere under interglacial conditions than it predicts. There is also the question of the real effect of whole ocean

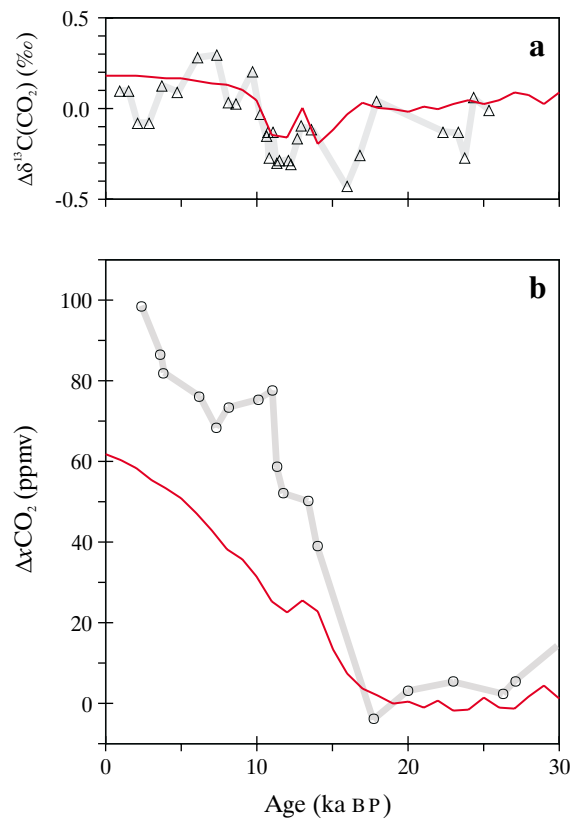


Figure 5-20 Evolution of atmospheric composition surrounding Termination I as a result of the composite scenario with improved temporal relationships of northern hemisphere forcing with respect to change in the southern hemisphere; (a) model $\delta^{13}\text{C}^{\text{CO}_2}$ (red line) with observations from the Taylor Dome ice core record [Smith *et al.*, 1999] (grey line with data points), (b) model $x\text{CO}_2$ (red line) with observations from the Vostok ice core record [Petit *et al.*, 1999] (grey line with data points).

aeolian deposition as opposed to the minimum case (i.e., Southern Ocean only) imposed in the composite scenario. It would not be unreasonable to assume that Fe fertilization could account for the missing intra-glacial variability in $x\text{CO}_2$, particularly since no other potential forcings share a similar pattern over this period. This would imply an additional ~15 ppmv at deglacial inception taking the initial rise to around 40 ppmv (only 10 ppmv short of that observed). The deficit in total CO_2 increase since the LGM would then be reduced to ~15 ppmv. Aside from model sensitivity to Fe availability, the temporal evolution of the global silica cycle also plays a role. Since the onset of H_4SiO_4 limitation in parts of the Southern ocean appears to be a key factor in the degree of CO_2 draw-down obtained, if the ocean inventory of dissolved Si is incorrectly predicted at the LGM then the magnitude of the effect of Fe fertilization may also be in error. Unfortunately, there are no reliable quantitative constraints available as to the state of the global silica cycle over the late Quaternary, leaving this as an unknown factor.

Perhaps more problematic to the composite scenario is the response of deep-sea sedimentary CaCO_3 . Preservation of CaCO_3 during glacial periods is over-predicted in the Pacific with a deepening of the calcite lysocline of ~ 1 km. Increased aeolian detrital supply to the deep ocean during glacial periods (e.g., Stages 2, 4, and 6) has a significant diluting effect on CaCO_3 content, indicated by a sharp shoaling of the depth of the lysocline. That this feature is not apparent in the lysocline evolution reconstruction of *Farrell and Prell* [1989] (if not an artefact of their relatively low core resolution and interpolation algorithm) may be a consequence of zonal averaging in the model. Mean detrital deposition to ocean zones in the model will be biased by a component of elevated dust fluxes near ocean margins, and thus will not be representative of the more remote location of many of the sediment cores used in lysocline reconstructions. Similarly, accepting some of the glacial lysocline shoaling as an artefact of model resolution places reconstructed sedimentary CaCO_3 changes in the Atlantic in first-order agreement with observations. The comparatively muted response of the CCD in both Atlantic and Pacific basins is in accordance with observations.

Interestingly, periods of peak detrital input aside, the thickness of the lysocline transition zone in the Pacific appears to be relatively invariant compared to that in the Atlantic. This suggests that Pacific CaCO_3 sediments are responding primarily to changes in ocean $p\text{H}$ rather than being controlled by changes in the CaCO_3 :POC rain ratio. The excessive excursions in lysocline depth in the Pacific together with over-estimated glacial CaCO_3 preservation thus indicates too great a change in deep ocean $p\text{H}$, which at the equator is some ~ 0.12 $p\text{H}$ units higher (3300 depth) during glacial times. This is in contrast to the increase of ~ 0.3 $p\text{H}$ units deduced via the $\delta^{11}\text{B}$ 'paleo-acidity' proxy in this region [*Sanyal et al.*, 1995, 1997]. If this proxy were to be correct then an even greater excursion in lysocline depth than that predicted would be expected. This apparent contradiction between evidence for glacial-interglacial changes in ocean chemistry deduced from sedimentary CaCO_3 and from boron isotopes has been a considerable puzzle in paleoceanography [*Archer et al.*, 2000; *Sanyal et al.*, 1995; *Sigman et al.*, 1998]. However, there is a substantial inter-specific vital influence on ^{11}B fractionation upon calcite deposition [*Sanyal et al.*, 1996; *Vengosh et al.*, 1991]. Benthic foraminiferal $\delta^{11}\text{B}$ measurements are made on mixed assemblages because of the analytical requirements of this method [*Sanyal et al.*, 1996, 1997]. Therefore, there is no guarantee that changes in bulk $\delta^{11}\text{B}$ represent changes in ambient ocean $p\text{H}$ as opposed to changes in species composition or even of the sedimentary environment [*Berger and Vincent*, 1986; *Mackensen et al.*, 1993; *Palmer et al.*, 1998]. If, for the sake of argument, the interpretation of $\delta^{11}\text{B}$ is taken to be correct, then deep waters in the Pacific during the last glacial were characterized by a carbonate ion content some ~ 100 $\mu\text{mol kg}^{-1}$ higher than at present [*Sanyal et al.*, 1995]. However, applying the least $[\text{CO}_3^{2-}]$ -sensitive dependence of foraminiferal ^{13}C fractionation observed by [*Spero et al.*, 1997] (2.2.6.4) would suggest that glacial ocean $\delta^{13}\text{C}^{\text{DIC}}$ was actually some $\sim 0.6\%$ higher than observed,

giving a net deglacial decrease in $\delta^{13}\text{C}^{\text{DIC}}$ of $\sim 0.3\%$. This completely contradicts all that is currently accepted regarding increased storage of carbon in the terrestrial biosphere since the LGM (5.4.6). Given that both proxies extrapolate planktonic fractionation behaviour to the benthic environment [*Spero et al.*, 1997], it would be difficult to entirely accept one whilst disregarding the other. It is, therefore, concluded that the $\delta^{11}\text{B}$ paleo-acidity proxy may well overestimate the magnitude of glacial-interglacial $p\text{H}$ change, perhaps by a factor of three. $[\text{CO}_3^{2-}]$ -dependent ^{13}C fractionation may be similarly overstated for the benthic environment.

In light of its poorly quantified envelope of operation, it is tempting to remove the 'coral reef hypothesis' from the composite scenario in order to meet criteria laid down by the paleoceanographic CaCO_3 record. Indeed, without this mechanism both modern and LGM-age CaCO_3 distributions in the model are consistent with reconstructions (not shown). However, intuitively it seems unlikely that rates of neritic CaCO_3 accumulation should have been largely invariant with respect to substantial changes in sea level and shelf area. However, it is possible that these effects were offset by decreased riverine supply of DIC and ALK (derived via continental weathering) during glacial periods. Although the 'coral reef hypothesis' produces a lagged response in $x\text{CO}_2$ at deglaciation, it is an important component in setting the overall sawtooth form of the glacial-interglacial cycles. It would therefore appear that a mechanism is required that enhances the underlying decline of $x\text{CO}_2$ as glacials deepen but does not drive deep ocean $p\text{H}$ overly high. Such a solution might lie in the long-overlooked phosphate extraction model. As an explanation for the entire magnitude of glacial-interglacial change this fell foul of timing issues together with considerations of oceanic $\delta^{13}\text{C}^{\text{DIC}}$ and dissolved oxygen changes [*Keir and Berger*, 1983; *Knox and McElroy*, 1984; *Shaffer*, 1990]. However, none of these need be violated if only a proportion of the total CO_2 draw-down is required. In the absence of parallel changes in the dissolved Si inventory of the ocean, only non-siliceous phytoplankton might generally be expected to be able to take advantage of increased PO_4 availability. This would lead to increased CaCO_3 export and thus the removal of DIC and ALK from the ocean, exerting a negative pressure on $p\text{H}$. Unfortunately, little is currently quantitatively understood with regards to deposition in the neritic environment and less still reliably known about the fate of interglacial-age sediments deposited there when sea level falls.

Finally, considering the problems discussed above regarding adherence to ocean chemical constraints, even in order to achieve only two thirds of the observed amplitude of glacial-interglacial $x\text{CO}_2$ variability, it is difficult to envisage a substantially larger change in terrestrial carbon inventory than the 500GtC considered so far, as has been proposed by some authors [*Adams et al.*, 1990; *Adams and Faure*, 1998; *Maslin et al.*, 1995].

5.7 The sequence of events surrounding Termination I

In light of the results from both the individual mechanisms tested and from the composite scenario, a conceptual sequence of events perturbing the global carbon cycle at deglaciation is proposed. Termination I is chosen for illustration. A sequence of transitional stages between the end of the LGM and the present-day (pre-industrial) is defined on the basis of identifiable paired trends in both $x\text{CO}_2$ and $\delta^{13}\text{C}^{\text{CO}_2}$ with additional constraints taken from the timing of The Antarctic Cold Reversal (ACR) and Younger Dryas (as delineated by observed variations in Vostok and GRIP CH_4 concentrations [Blunier *et al.*, 1997], and from the recent results presented from DOME C by Monnin *et al.* [2001]). Marine Isotope Stage 1 is subdivided for illustration, something akin to that for Stage 5. The proposed sequence of events surrounding Termination I is as follows (Figure 5-21):

Stage 2. Full glacial conditions. High rates of dust supply to the Southern Ocean (although already starting to decline towards the end of this period). Generally iron replete conditions with a dominance of siliceous phytoplankton in the determination of POC export production. Low levels of $x\text{CO}_2$ and intermediate $\delta^{13}\text{C}^{\text{CO}_2}$.

Stage 1g. Dust deposition to the Southern Ocean decline rapidly and iron starts to limit export production leading to a rise in $x\text{CO}_2$. A combination of decreased productivity together with a shift in ecosystem composition towards non-siliceous species (which fractionate ^{13}C in organic matter less strongly) results in a drop in $\delta^{13}\text{C}^{\text{CO}_2}$ concurrent to the $x\text{CO}_2$ rise. The negative trend in atmospheric isotopic signature is exacerbated by a collapse of the maximum seasonal limits of sea ice extent in the Southern Ocean, perhaps driven by a combination of increasing local temperature and relatively high austral summer insolation levels at 65°S at this time [Jouzel *et al.*, 1987, 1995; Laskar *et al.*, 1993]. Slightly offsetting the negative excursion in $\delta^{13}\text{C}^{\text{CO}_2}$ but enforcing the $x\text{CO}_2$ rise during this stage are increasing SSTs in the southern hemisphere.

Stage 1f. Dust decline is virtually complete, with Southern Ocean productivity at near-interglacial levels. There is a much slower rise in CO_2 levels, perhaps due to increases in carbon stored in the terrestrial biosphere, particularly in the tropics and in the SH offsetting the effect of increasing SSTs. Together these two effects constructively interfere to force $\delta^{13}\text{C}^{\text{CO}_2}$ to start to rise.

Stage 1e. Bölling/Alleröd. The northern hemisphere now starts to deglaciate, with substantial ice sheet collapse. Rapidly rising SSTs in the NH together with an intensification of the Atlantic overturning circulation drive CO_2 levels higher. This is later compensated for by lower SH SSTs during the ACR [Blunier *et al.*, 1997; Smith *et al.*, 1999] producing a slight decline towards the end of this stage. Initial continuing increases in $\delta^{13}\text{C}^{\text{CO}_2}$ also reflect the sudden change in NH climate and

increases in terrestrial biome carbon storage (although it is not immediately obvious what might subsequently produce the slight decline observed).

Stage 1d. Younger Dryas. Return to near-LGM conditions in the North Atlantic region. Atmospheric CO_2 concentrations increase again following the end of the ACR event. Reductions in carbon stored in the terrestrial biosphere could produce further increases in $x\text{CO}_2$ while reducing $\delta^{13}\text{C}^{\text{CO}_2}$, as observed.

Stage 1c. Deglaciation restarts. Similar initial forcings on the system as per Stage 1e. Global climate attains typical interglacial conditions. Further increases in $\delta^{13}\text{C}^{\text{CO}_2}$ throughout this stage driven by higher SSTs in both hemispheres together with greater terrestrial biome carbon storage. After the initial rise there is a gradual reduction in $x\text{CO}_2$ possibly a result of the continued expansion of terrestrial ecosystems, particularly in northern subtropical regions [Brovkin *et al.*, 1998; Claussen and Gayler, 1997; Indermühle *et al.*, 1999].

Stage 1b. Collapse of sub-tropical ecosystems with a slight cooling in climate, leading to a significant fall in $\delta^{13}\text{C}^{\text{CO}_2}$ over the course of this stage, with reduced terrestrial biomass dominating over SST effects to bring about an increase in $x\text{CO}_2$ [Indermühle *et al.*, 1999].

Stage 1a. Slight decrease in $x\text{CO}_2$ with an increase in $\delta^{13}\text{C}^{\text{CO}_2}$ despite no significant climatic change occurring during this interval, perhaps as a result of the expansion of northern hemisphere peatlands [Klinger *et al.*, 1996].

Changes in the oceanic CaCO_3 system (i.e., 'carbonate compensation' and neritic CaCO_3 storage) and dissolved Si cycles have not been discussed in the above. While these have time constants of change too long for them to be directly involved in some of the observed rapid variations in the sign of change of atmospheric composition, they will be important in determining the overall deglacial trend.

Supporting the causal linkage between dust supply and $\delta^{13}\text{C}^{\text{CO}_2}$ suggested to account for part of the Stage 1g anomaly are records presented by Ninnemann and Charles [1999] of planktonic foraminiferal $\delta^{13}\text{C}$ from the Southern Ocean. Not only do these exhibit a prominent negative excursion consistent with the Taylor Dome record [Smith *et al.*, 1999] following the dust decline at the end of Stage 2, but also a (slightly smaller) negative excursion at around 60 ka BP, apparently synchronous with the earlier substantive drop-off in dust deposition (as recorded in the Vostok core [Petit *et al.*, 1999]). Additional paleoceanographic evidence that changes in productivity drive at least part of the Stage 1g $\delta^{13}\text{C}^{\text{CO}_2}$ excursion comes from benthic foraminiferal $\delta^{13}\text{C}$ records from the South Atlantic [Charles *et al.*, 1996]. These show prominent negative anomalies, synchronous both with initial rise in local SST (itself synchronous with Vostok δD) and again, also with the Stage 3/4 boundary.

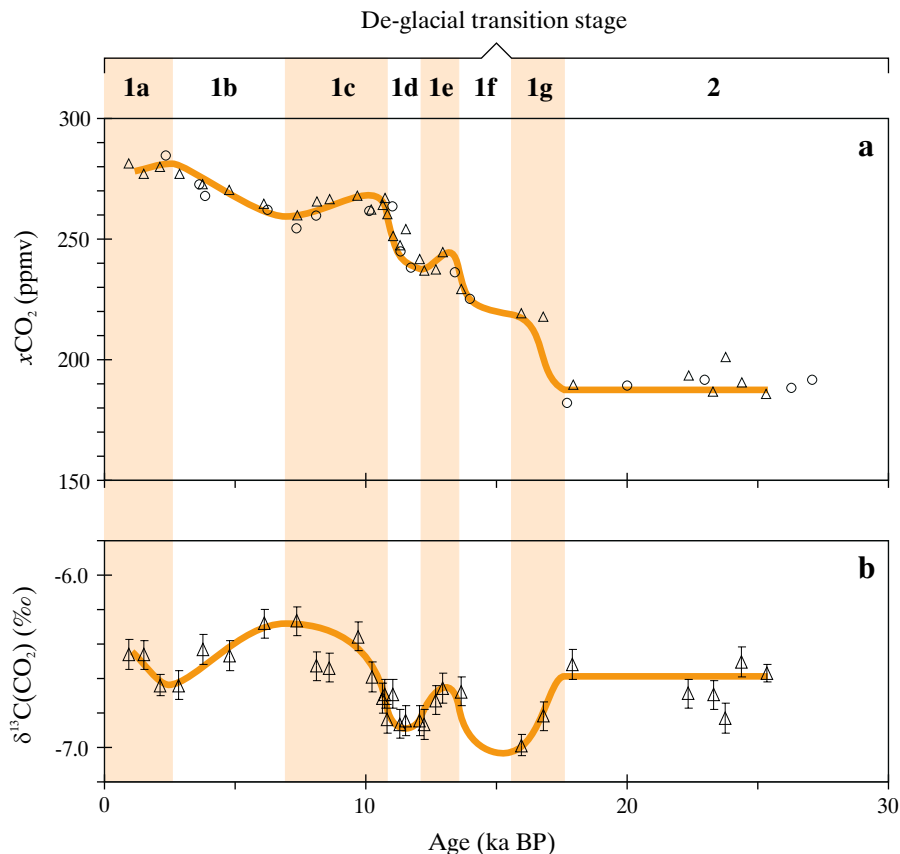


Figure 5-21 Conceptual transition stages in the global carbon cycle surrounding Termination I; (a) observed atmospheric CO₂ concentration records from the Vostok [Petit *et al.*, 1999] (circles) and Taylor Dome [Smith *et al.*, 1999] (triangles) ice cores placed on the Vostok chronology as described previously (5.2), with suggested general trends indicated by the orange line, (b) observed δ¹³C^{CO₂} record from the Taylor Dome [Smith *et al.*, 1999] (triangles) ice core, with suggested general trends again indicated.

5.8 What ultimately drives the deglacial rise in atmospheric CO₂?

Should the onset of Fe limitation in the Southern Ocean brought about by a decline in dust deposition to this region be the primary driving force behind the initial deglacial increase in atmospheric CO₂ levels, what might cause dust to decline in the first place? The mechanisms driving dust variability are especially intriguing since at each glacial termination the decline appears to precede significant changes in other indicators of southern hemisphere climate (such as ice core δD and xCO₂) by some ~5 ka. The interval is as great as 10 ka with respect to northern hemisphere ice sheet collapse [Broecker and Henderson, 1998]. A clue comes from the apparent correlation between periods of rapid sea level fall and peak dust deposition fluxes (Figure 5-22), at least over the last ~250 ka (before which the SPECMAP and Vostok time scales diverge). Furthermore, dust starts to decline slightly prior to the stabilization of sea level at local minima.

Mineralogical and isotopic analysis suggest that the primary source area for dust deposited at Vostok during the LGM was Patagonia [Grousset *et al.*, 1992]. The effective land area of this region would have been substantially enhanced during glacial periods of low sea level stand through the exposure of the adjoining continental shelves [Iriando, 2000]. Unconsolidated shelf sediments could have been easily deflated and transported by the prevailing winds out across the Southern Ocean [Iriando, 2000]. The simplest explanation for the apparent relationship between sea level and Vostok dust fluxes would then be that dust supply is directly related to exposed shelf area. However, assuming dust fluxes in proportion to this area (derived from mean ocean bathymetry lying between 20°S and 70°S [ETOPO5, 1988], encompassing the Patagonian region [Basile *et al.*, 1997]) produces a response that bears little resemblance to the Vostok record. On the basis that dust source regions have a finite lifetime after which they become effectively completely deflated [Pye, 1989; Rea, 1994], the source strength of each portion of shelf newly exposed is relaxed. With a characteristic decay rate of 0.1 ka⁻¹, a series of sharp peaks is obtained lying atop of a background (not shown).

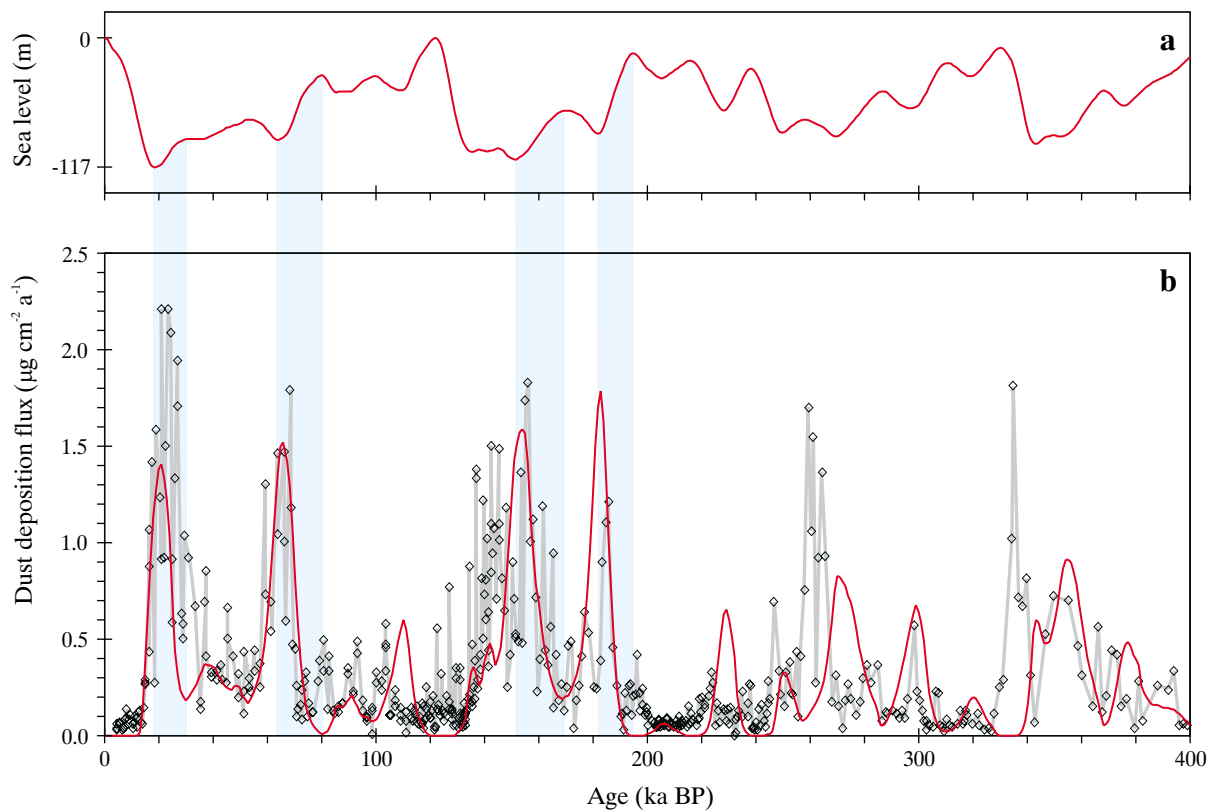


Figure 5-22 Idealized dust flux model based on changes in exposed shelf area in the mid and high southern hemisphere latitudes. Shown are (a) sea level history reconstructed from the SPECMAP $\delta^{18}\text{O}$ stack [Imbrie *et al.*, 1984] and assuming a 117 m rise rise the LGM [Fairbanks, 1989], (b) the Vostok dust deposition flux record [Petit *et al.*, pers comm] (grey line with data points) together with model results (red line). Periods of rapid sea level fall of particular interest are highlighted.

Although the timing of these peaks is in excellent agreement with Vostok, since their heights relate directly to the rate and overall magnitude of each fall in sea level, the strongest dust peak is predicted to occur with the Stage5e/5d transition, contrary to the Vostok record. One final adjustment is now made to the model: since a warm wet climate is conducive to vegetation cover and will hinder atmospheric dust transport [Yung *et al.*, 1996], account must be taken of the gradual climatic transition into cold dry glacial conditions. Model dust fluxes are therefore arbitrarily weighted by the square of SPECMAP (normalized to a value of unity at 19 ka BP). The result of this final model is shown in Figure 5-22. It can be seen that not only can the relative heights and timing of the major dust peaks be reproduced, so can background trends. For the Stage 4 and 2 dust peaks in particular, the respective phases of declining dust fluxes between model and observations correspond to within ~ 1 ka.

Despite the surprising success of such a simple model, recent studies of the provenance of dust deposited in Antarctic ice casts some doubt on this shelf dust source hypothesis. Detailed geochemical analyses based on the Rb-Sr and Sm-Nd isotopic systems put the primary source regions of dust deposited in East Antarctica as Patagonian

loess rather than sediments lying on the Argentine continental shelf [Basile *et al.*, 1997]. Although this suggests that sea level fall cannot directly control dust sources through shelf exposure, the apparent linkage between periods of rapid change as delineated by the SPECMAP $\delta^{18}\text{O}$ record [Imbrie *et al.*, 1984] and peak dust concentrations still requires an explanation. A second hypothesis is therefore advanced, in that during periods of ice sheet advance the supply of glacially-eroded material (particularly fines such as rock flour) fuels the overall rate of dust deflation from Patagonia. In such a scenario, supply falls off as active erosion of new regions ceases with the stabilization of ice extent, with the result that dust fluxes start to decline just as peak glacial conditions are attained, as observed.

Sudden increases in the concentration of atmospheric CO_2 in the atmosphere could thus be a consequence of glaciological dynamics. That deglaciation occurs following Stage 2 rather than Stage 4 may be due to a critical glacial extent having been attained in Patagonia, analogous to the ‘excess ice’ hypothesis [Paillard, 1998; Raymo, 1997; Ridgwell *et al.*, 1999], with the catastrophic collapse of dust supply at the end of Stage 2 perhaps occurring as glaciers reach the ocean margin or extend beyond regions rich in erodible

material. Whatever the ultimate cause of dust variability, declining deposition rates to the Southern Ocean is the only mechanism that clearly precedes $x\text{CO}_2$ rise, strongly implicating it in the initial deglacial perturbation of the global carbon cycle and thus in the dynamics of the 100 ka ice age cycles of the late Quaternary.